FRA-74-6
REPORT NO. FRA-ORD&D-75-6

LATERAL STABILITY OF A DYNAMIC RAM AIR CUSHION VEHICLE

Paul V. Aidala

AUGUST 1974

FINAL REPORT

Prepared for

U.S. DEPARTMENT OF TRANSPORTATION
FEDERAL RAILROAD ADMINISTRATION
Office of Research, Development and Demonstrations
Washington DC 20590

Technical Report Documentation Page

1. Report No.	2. Government Accession No.	3. Recipient's Catalog No.
FRA-ORD&D-75-6		

4. Title and Subtitle	5. Report Date
LATERAL STABILITY OF A DYNAMIC RAM AIR CUSHION VEHICLE	August 1974
	6. Performing Organization Code
7. Author(s)	8. Performing Organization Report No.
Paul V. Aidala*	DOT-TSC-FRA-74-6
9. Performing Organization Name and Address	10. Work Unit No. (TRAIS)
M.I.T., Aerophysics Laboratory 560 Memorial Drive Cambridge MA 02139	RR418/R4334
	11. Contract or Grant No.
	DOT-TSC-239
12. Sponsoring Agency Name and Address	13. Type of Report and Period Covered
U.S. Department of Transportation Federal Railroad Administration Office of Research, Development and Demonstrations Washington DC 20590	Final Report November 1, 1972 to May 31, 1974
	14. Sponsoring Agency Code

15. Supplementary Notes

*Under Contract to: U.S. Department of Transportation, Transportation Systems Center, Kendall Square, Cambridge MA 02142

16. Abstract

The lateral stability derivatives of a dynamic ram air cushion vehicle in a rectangular guideway were measured using a ship model towing tank. Lift and pitching moment are also reported. The primary lateral derivatives are all stabilizing, with significant cross coupling in some cases. The longitudinal forces are compared with the numerical prediction of the one-dimensional mass conservation theory given by Boccadoro, with good agreement. A trailing edge Trefftz analysis is presented and used to predict the lateral derivatives. Comparison with the lateral data is good for side displacement derivatives but is less successful for yaw angle derivatives. The towing tank is found to be an effective method for testing dynamic air cushion vehicles.

17. Key Words	18. Distribution Statement
Vehicle, ram-wing: test, towing-tank Dynamic air cushion Ram air cushion TRACV	DOCUMENT IS AVAILABLE TO THE PUBLIC THROUGH THE NATIONAL TECHNICAL INFORMATION SERVICE, SPRINGFIELD, VIRGINIA 22151.

19. Security Classif. (of this report)	20. Security Classif. (of this page)	21. No. of Pages	22. Price
Unclassified	Unclassified	72	

Form DOT F 1700.7 (8-72) Reproduction of completed page authorized

PREFACE

The work described in this report represents part of an ongoing effort to develop a high speed ground transportation vehicle utilizing aerodynamic forces for suspension. Small scale model demonstrations of this concept were carried out at Princeton University as early as 1965, and low level efforts have been carried out at the Massachusetts Institute of Technology and elsewhere since then. A recently completed system definition study has investigated the merits of this concept and defined the characteristics of a complete ram air cushion vehicle and guideway. The Federal Railroad Administration has funded this program for the past five years, through the Office of Research Development, and Demonstrations.

The present report documents recent experimental results. A trailing edge Trefftz analysis is presented as a method to predict the lateral derivatives. Additional theoretical efforts are summarized in a separate report.

TABLE OF CONTENTS

LIST OF ILLUSTRATIONS

LIST OF ILLUSTRATIONS (continued)

SYMBOLS

AR	aspect ratio = $\frac{b}{c}$	
b	width or span of model	
c	length or chord of model	
C_ℓ	rolling moment coefficient	$C_\ell = \frac{\ell}{(\hat{q}\hat{b}\hat{c})\hat{b}/2}$
C_L	lift coefficient	$C_L = \frac{L}{\hat{q}\hat{b}\hat{c}}$
C_M	pitching moment coefficient	$C_M = \frac{M}{(\hat{q}\hat{b}\hat{c})\hat{c}}$
C_N	yawing moment coefficient	$C_N = \frac{N}{(\hat{q}\hat{b}\hat{c})\hat{b}/2}$
C_Y	side force coefficient	$C_Y = \frac{Y}{\hat{q}\hat{b}\hat{c}}$
G	rolling moment axis z-coordinate	
K_n	integration constant, n integer	
ℓ	rolling moment	
L	lift	
m	mass flux	
M	pitching moment about midchord	
N	yawing moment about midchord	
p	pressure	
Q	complex velocity (Appendix B)	
q	dynamic pressure, q = 1	$\hat{q} = \frac{1}{2}\hat{\rho}\hat{U}^2$
r	λ/λ_o	
s	λ_o/ε	

SYMBOLS (continued)

t	length of model side at trailing edge
U,V,W	linear velocities about x,y,z. $U = 1$ $\hat{U}$ = model velocity
v_L	"sidewash" of left side of model, $v_L = v_o + \psi$
v_o	"sidewash" due to taper of model sides
v_R	"sidewash" of right side of model, $v_R = v_o - \psi$
w_o	downwash of model. $w_o = \alpha$ in the present experiment
x_o	midchord point
Y	side force
α	angle of attack
Γ	circulation
ε	trailing edge vertical clearance
λ	side displacement at midchord of lips plane
λ_o	nominal side gap
λ_L	Λ_L at trailing edge $\lambda_L = \lambda_o + \lambda - \psi x_o$
λ_R	Λ_R at trailing edge $\lambda_R = \lambda_o - \lambda + \psi x_o$
Λ	generalized side gap (Appendix B)
Λ_L	left side gap, $\Lambda_L = \lambda_o + \lambda - \psi(x - x_o)$
Λ_R	right side gap, $\Lambda_R = \lambda_o - \lambda + \psi(x - x_o)$
ρ	fluid density
ϕ	roll angle
ψ	yaw angle
ω	ε/Λ (Appendix B)

SYMBOLS (continued)

$(\hat{})$	dimensional variable (unsuperscripted variables are dimensionless)
$(...)_{\lambda,\psi,...}$	derivative with respect to the variable used as subscript

Lengths are nondimensionalized by the semispan, $\hat{b}/2$.

Model Parameters

span	$b=2$	$\hat{b}=11.505$ inches
chord	$c=6.91$	$\hat{c}=39.75$ inches
rolling moment axis z-coordinate	$G=0.087$	$\hat{G}=0.5$ inches
height of side at trailing edge	$t=0.782$	$\hat{t}=4.50$ inches
taper of model sides	$v_o=0.028$	
nominal side gap	$\lambda_o=0.0435$	$\hat{\lambda}_o=0.25$ inches
roll angle of experiment	$\phi = \pm 0.0785$	$\hat{\phi} = \pm 4.5$ degrees

1. INTRODUCTION

The study of the Tracked Ram Air Cushion Vehicle (TRACV) has been motivated by the concept of using aerodynamic lift as a means of suspension for high speed ground transportation. Earlier terminology labeled a TRACV a "ram wing" in view of the "ram" pressure developed beneath the vehicle from the momentum of the incoming fluid. Previous analytical investigations have used pertubation analysis to develop the velocity potential (1, 2, 3). Experiments by Pepin (4, 5) have verified the results of pertubation analysis of a TRACV, and revealed the limitations imposed by the necessary ordering assumptions.

Other experimental investigations have shown that one-dimensional mass continuity can be used to predict the longitudinal forces on a TRACV (6, 7, 8). More recently, the TRACV lateral dynamics have been emphasized (7, 8, 9, 10, 11) in order to evaluate vehicle-guideway interactions for a tracked air cushion vehicle. Analytical solutions for a flat plate with a roll angle in a guideway have been derived using

pertubation series expansions (9, 10, 11). Analysis of the forces due to side displacement of a vehicle in a guideway are developed in the present report.

The research described herein consists of two parts: an extension of the experiment initiated by Boccadoro (8), and the development of an analytical procedure to predict the lateral forces. The experimental objectives were to measure the static lateral derivatives of a TRACV in a guideway and to evaluate the towing tank method as an experimental procedure. Lift and pitching moment on the vehicle are also reported and compared with that predicted by the one-dimensional analysis of Boccadoro (8). Good agreement is shown. It was also found that the primary lateral derivatives were all stabilizing; that is, positive side displacement generates a negative side force, positive roll angle a negative rolling moment, and positive yaw angle creates a negative yawing moment. Cross-coupling derivatives were also measured and found to be of large magnitude in some cases. Side force and rolling moment were predicted using a Trefftz plane analysis described in Chapter 2. The analysis shows good agreement with the data for side displacement derivatives. The prediction of the forces due to yaw angle is less successful than the prediction of the forces due to side displacement. The attempt to predict roll angle derivatives is completely unsuccessful.

The results obtained show that the towing tank is an effective method for testing a ground effect vehicle in a guideway.

evaluated for the model with no side displacement, mathematical singularities develop. These occur because the sharp corner of the model image used in Figure 2.1 contacts the side wall for the roll angle of the experiment with no side displacement. When a corner and wall touch, the argument of some of the logarithmic expressions becomes zero. (The rounded corners on the actual model would not contact the wall for zero side displacement.) If a side displacement was included in order to avoid the singularity, force predictions greatly in excess of the measured values result. More detailed analysis for a rolled vehicle is necessary.

It should be noted that this type trailing edge analysis cannot be used to predict the lift on the model. This is due to the presence of the two vortices developing at the edges of the lip plane of the vehicle as is typical for a low aspect ratio wing. The lift contribution of these vortices has been called the "cushion lift" for a TRACV (10) but their influence on the lateral derivatives is uncertain. They have been entirely neglected in the preceeding analysis by imposing the condition $\Gamma = 0$ at the tips ($z = t$).

The lift could be increased by adding a constant to Γ to satisfy a non-zero boundary condition at $z = t$, keeping the lateral forces unchanged. It would be expected

for an asymmetrical model configuration that the circulation at the tips would also be asymmetrical (i.e., $\Gamma_L(t) \neq \Gamma_R(t)$). Part of the failure of the trailing edge analysis for a rolled vehicle may be due to the neglect of a nonconstant circulation at the lips, although apparently it is less serious to neglect this effect in predicting the lateral forces for side displacement and yaw.

3. DESCRIPTION OF THE EXPERIMENT

3.1 General

The previous towing tests by Boccadoro identified two major problems: electronic and vibration noise in the force signals and poor accuracy in monitoring the position of the model. Improvements to the experiment concentrated on these two areas. This chapter describes changes to Boccadoro's experiment. The guideway, model and towing facilities remained identical. A more complete description of the original experiment will be found in Reference 8.

3.2 Position Transducers

Previously, five non-contacting eddy current sensors monitored both model clearance and side displacement. It was found that the close proximity of the several sensors resulted in an interaction between the height and side displacement measurements. For the present tests only three smaller transducers (0.75 inch diameter) of the same type were used. They were mounted close to the lips, one near

the leading edge of the model and two immediately behind the trailing edge. The two transducers at the trailing edge measured the model side displacement and the guideway width. The forward transducer monitored model yaw. Figures 3.1 and 3.2 show the transducer locations.

No transducers were used to monitor the vertical clearance. Previous tests showed that the model had very low sensitivities to changes in vertical position. The clearance was measured with spacers when the model was stationary.

A small section of guideway was built to allow calibration of the sensors in the model. A "calibration frame" was assembled in which the model and guideway section could be submerged in a small tank of water. Spacers were used to calibrate the sensors in the calibration frame and during testing. Figure 3.3a shows the model at a roll angle in the calibration guideway. Figure 3.4 is a schematic drawing of the guideway cross section.

The linear range of the transducers was 0 to .25 inches, with a sensitivity of four volts per inch. When installed on the model, the transducers were adjusted in their mountings to extend approximately .06 inches beyond the lip. Thus, the transducers were within their linear range when the side gap was the nominal .25 inches. The mounting offset was measured by fitting .25 inch spacers around the model in the guideway and reading the output of the sensors.

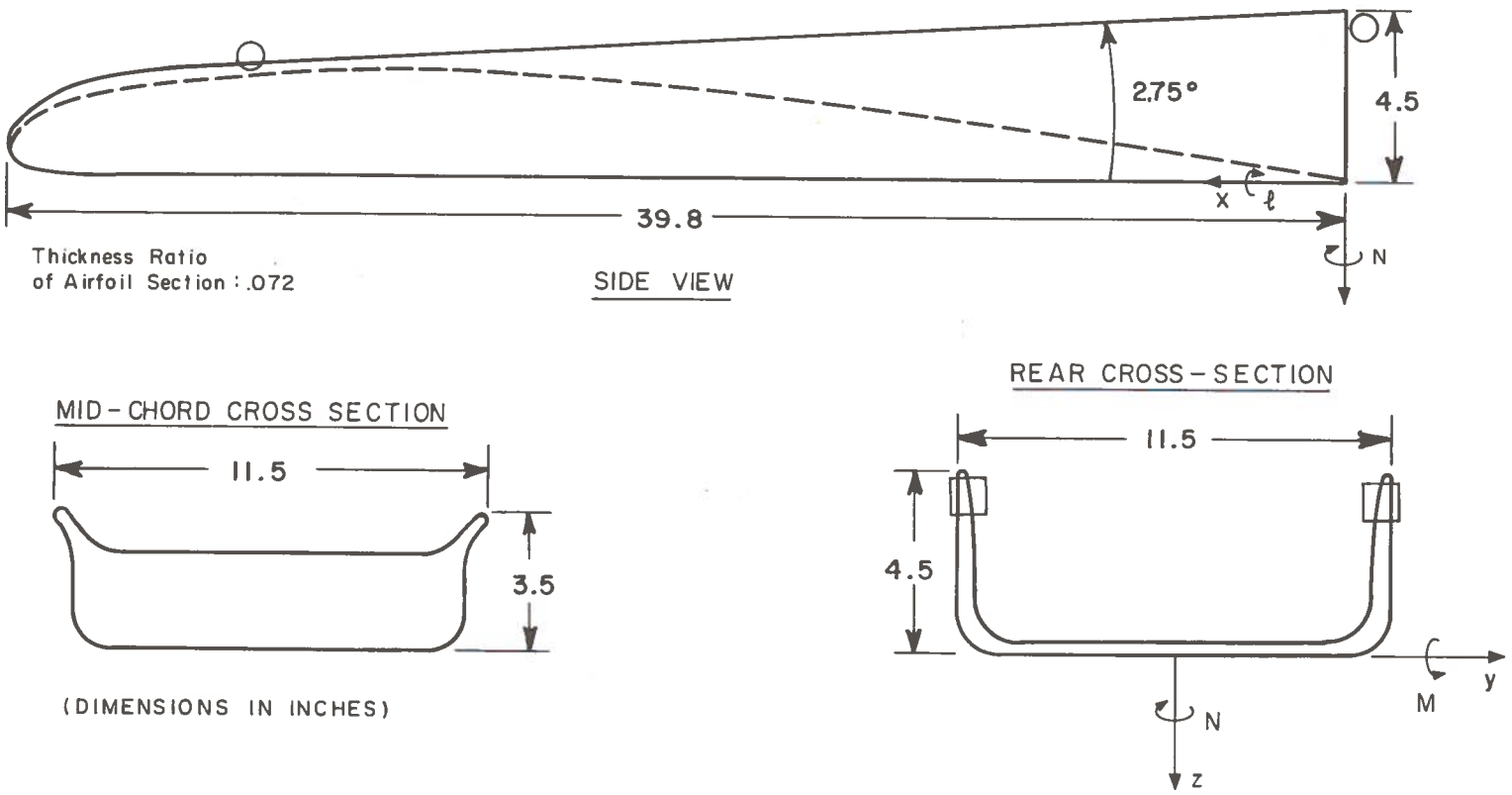

Fig. 3.1 Schematic Drawing of Model

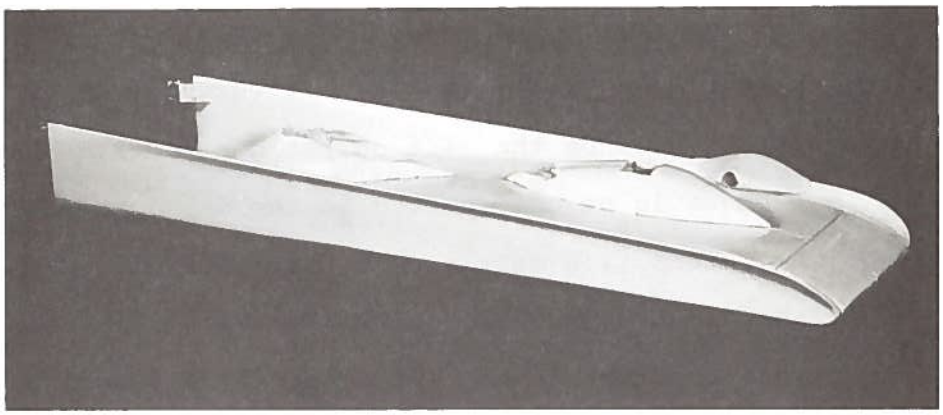

Fig. 3.2a Side View of Model

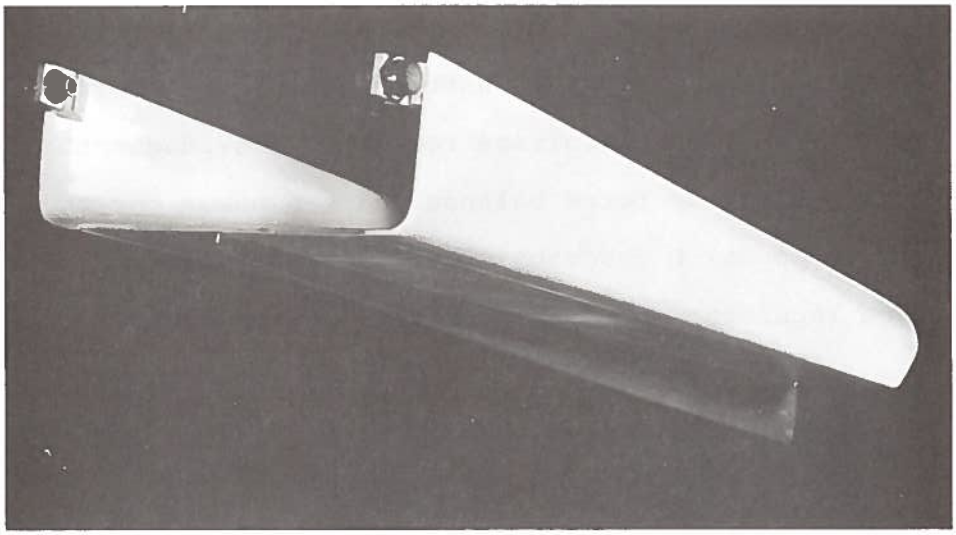

Fig. 3.2b Rear View of Model with Keel

3.3 Force Balance

The six-component force balance was the same as used by Boccadoro. Calibrations for the current tests revealed a very large interaction on the lift output due to drag. While this effect could be compensated in the data processing by means of the interaction matrix, its existence tended to reduce confidence in the results. After some investigation it was found that the interaction was caused by a pitching moment about the forward support of the balance. A moment is generated by a drag force applied either to the balance directly or to the supporting struts. A stainless steel brace was silver soldered to the balance to reduce the interaction. The balance in the model is shown in Figure. 3.5.

3.4 Signal Processing

Special D.C. amplifiers were built to process the force balance signals. A voltage regulator provided both the excitation for the force balance and the power for the amplifier. Appendix D describes the amplifier circuit. The voltage regulator and amplifier were mounted on the carriage.

The force signals from the amplifier were recorded on a multichannel Visicorder. The pressure and position signals were recorded on a separate chart. The two recorders were synchronized by having one of the position

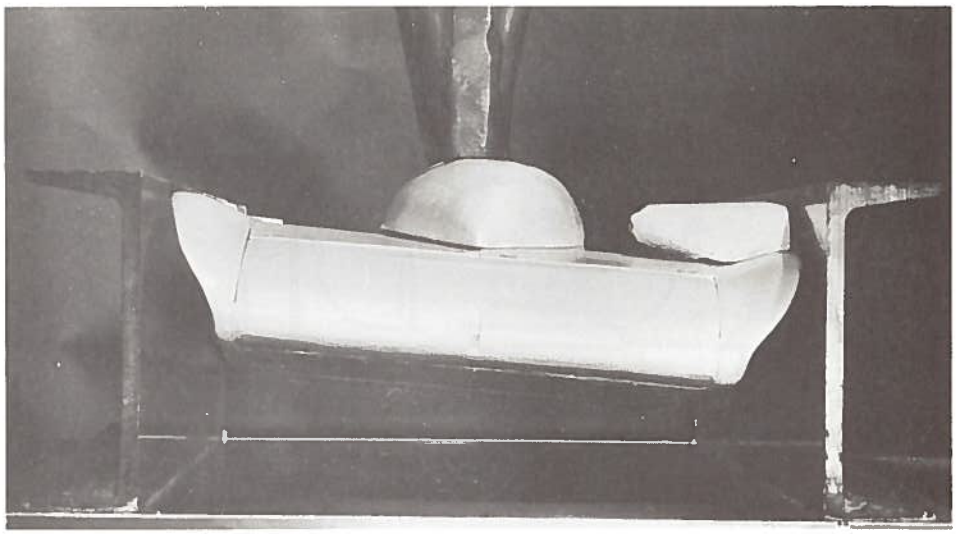

Fig. 3.3a Cross Section of Model in Calibration Guideway

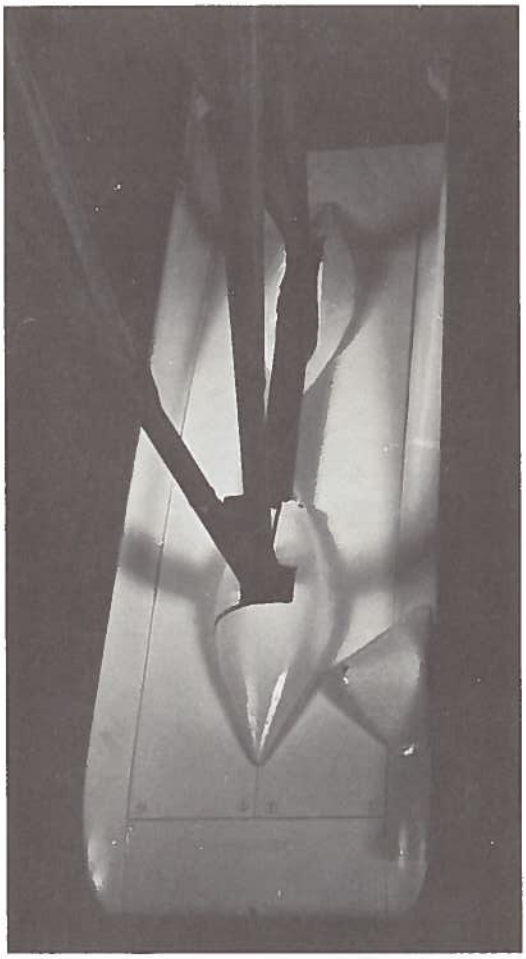

Fig. 3.3b Overhead View of Model Mounted on Supports

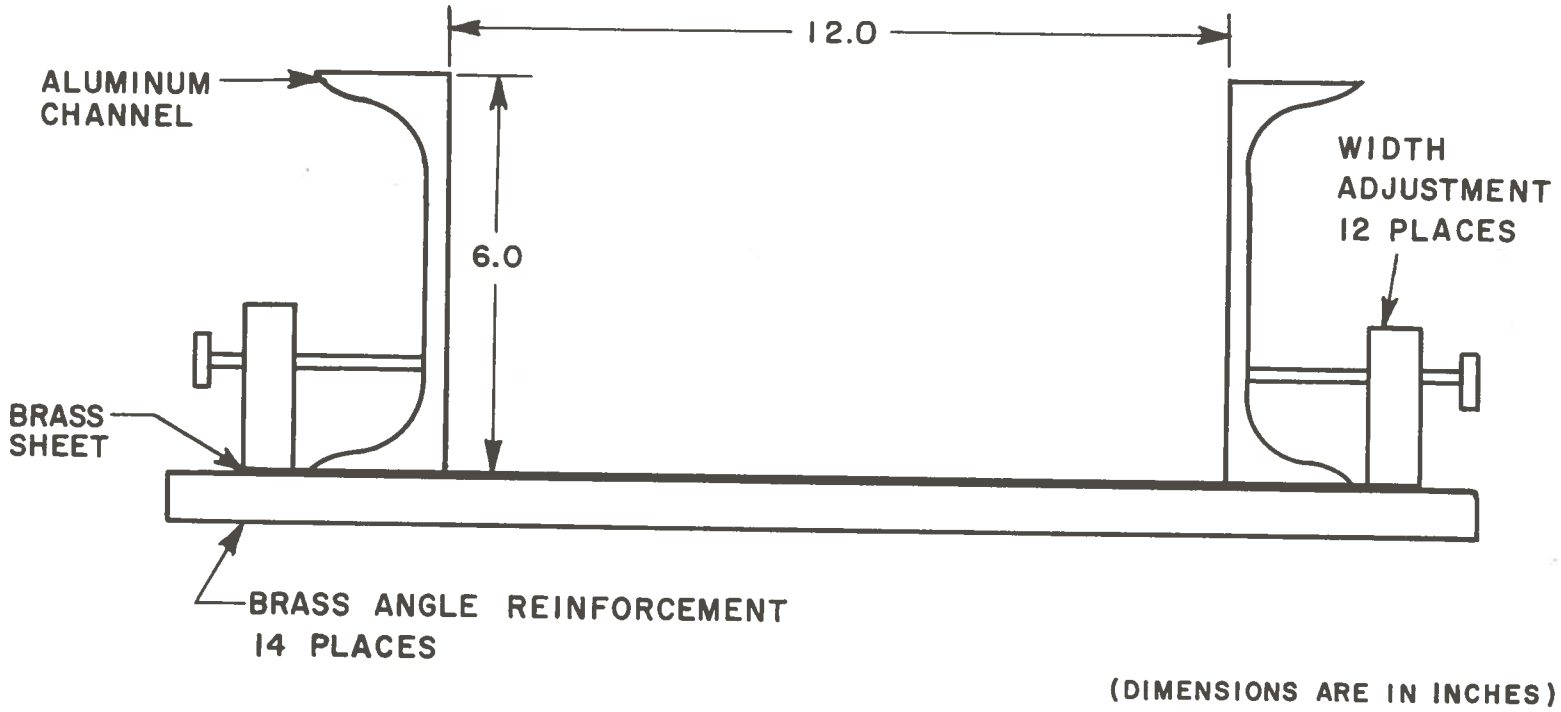

Fig. 3.4 Schematic Drawing of Guideway Cross Section

signals recorded on both devices. The transducers, recording instruments and amplifier circuit are described in Appendix D.

After insertion of the brace, the interaction matrix for these tests was

$$\begin{bmatrix} FL \\ AL \\ R \\ FS \\ AS \\ D \end{bmatrix} = \begin{bmatrix} 1 & 0.08 & 0 & 0 & 0 & -.38 \\ 0 & 1 & 0 & 0 & 0 & 0 \\ -.21 & 0 & 1 & 0 & 0 & 0 \\ .014 & 0 & 0 & 1 & -.16 & .20 \\ 0 & 0 & 0.006 & -.18 & 1 & -.015 \\ .026 & 0.056 & 0.02 & 0 & 0 & 1 \end{bmatrix} \times \begin{bmatrix} FL_o \\ AL_o \\ R_o \\ FS_o \\ AS_o \\ D_o \end{bmatrix}$$

where

FL = forward lift force, pounds

AL = aft lift force, pounds

R = rolling moment, inch-pounds

FS = forward side force, pounds

AS = aft side force, pounds

D = drag force, pounds

and

FL_o, AL_o, etc., are the readings from the recording device, expressed as pounds or inch-pounds.

3.5 Towing Carriage

The displacement sensors were used to check the guideway alignment. Towed at low speeds, the sensors showed a low frequency oscillation of the model in yaw.

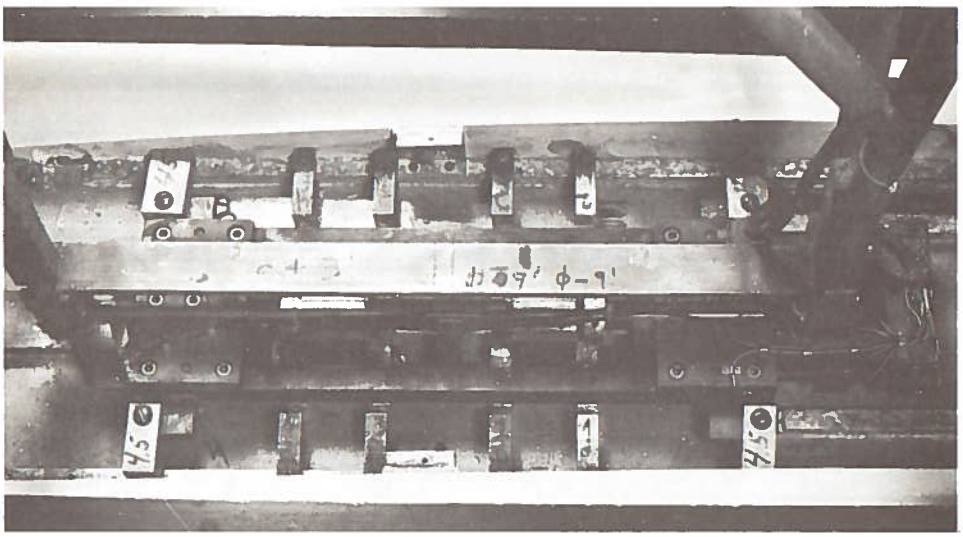

Fig. 3.5 Force Balance Inside Model

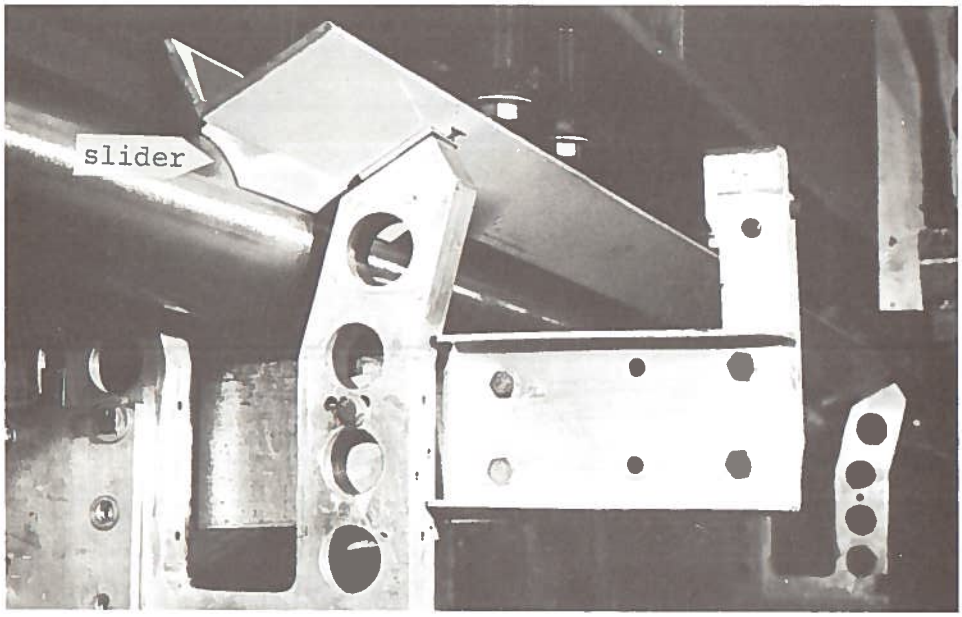

Fig. 3.6 Carriage Rail Slider

Eccentricities of the carriage wheels were the cause, which would become 6 Hz vibration noise at a test speed of 3 feet per second. To reduce vibrations, teflon sliders were made to replace the carriage wheels. Figure 3.6 shows one of the carriage sliders. In addition, the model supports were changed to mount the model below the center of the carriage, minimizing yaw deflections due to misalignments in the carriage rails. The speed of the carriage was frequently checked with two photo cells and a counter.

With the teflon sliders, towing the model at low speeds revealed several locations where misalignments of the carriage rails gave the model a yaw or side displacement. The rails were adjusted at two locations to improve the path of the model through the guideway.

3.6 Pressure Transducer

A small pressure transducer was mounted in one side of the guideway to record the pressure signature of the model. The pressure transducer was located such that the forward position sensor would provide a synchronizing pulse to locate the trailing edge in the pressure signal. The pressure transducer was usually mounted .5 inches from the bottom of the guideway. When the angle of attack was 2.75 degrees, the lip plane of the model became horizontal. Additional runs with .5 inches clearance were then made with the transducer located either approximately .3 inches above or .3 inches below the lip plane.

3.7 The Model

A schematic drawing of the model is shown in Figure 3.1. Several views of the model are shown in Figures 3.2 and 3.3. The model was mounted on the balance by four transverse beams attached to two cylindrical hinge pieces, which clamped onto the center beam of the force balance. The hinges allowed rotation of the model about the roll axis. A predetermined roll angle could be set by installing appropriately machined pieces at the corners of the balance. Figure 3.5 shows the balance with the model mounted for a roll angle of +4.5 degrees. The tolerance of the roll angle was less than .2 degrees.

Keels for a model vertical clearance of .5 inches and angles of attack of 2.0, 2.75 and 3.0 degrees were made. A notch in the leading edge of the model and two small bolts secured the keel to the model. A thin coating of silastic was put on the top edge of the keel to improve the seal with the undersurface of the model. The keels were designed for a nominal clearance of .025 inches between the bottom of the keel and the guideway. Figures 3.7 and 3.2 show the model with a keel attached.

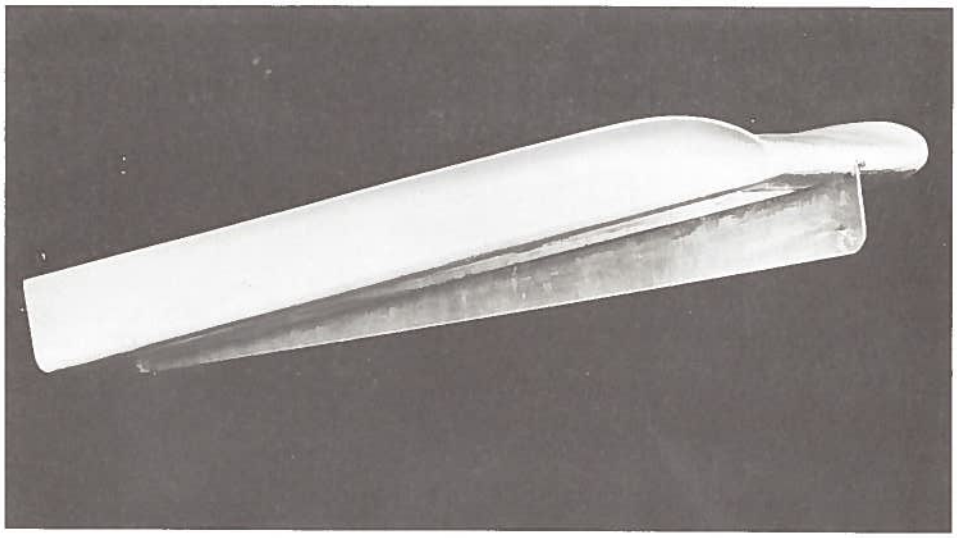

Fig. 3.7 Side View of Model with Keel

4. DISCUSSION OF THE RESULTS

4.1 General

The changes described in Chapter 3 developed from the difficulties of the earlier tests by Boccadoro. For the test reported here, equipment performance was very satisfactory. The largest remaining problem is the misalignment of the carriage rails, which gives the model a crooked path with respect to the guideway. The side displacement and yaw angle varied as the model traveled through the guideway. (The signal filtering prohibited the collection of dynamic information.) Data for the primary derivatives was tabulated from two locations in the guideway. Both the side displacement and yaw angle differed at the two locations. Thus, data from each run included the effects of both yaw angle and side displacement. Although it was felt that the data reduction techniques employed did manage to separate out the two effects, it would have been preferable to vary them separately.

4.2 Guideway

The position sensors monitored the side gap to ± .012 inches, 5% of the nominal side gap. Yaw angle was measured to less than .001 radians. A typical position recording is shown in Figure 4.1.

With respect to the model path, the straight line tolerance of the guideway walls was ± .060 inches. The tolerance of the guideway width was ± .025 inches in the first half of the test section and ± .010 inches in the second half (± .038 inches overall). The poor "straight line" tolerance of the guideway walls reflects the misalignments of the carriage support rails (i.e., the path of the model is not straight).

In the first half of the test section the guideway was .03 inches wider. Both λ, the displacement from the center of the guideway, and λ_o, the symmetrical component of the side gap, were increased. The change in λ_o affects mainly the lift. As expected, the lift was greater for the smaller side gap, but not enough for any quantitative conclusions. The change in λ_o was less than 6%, and was taken to always be the nominal side gap of .043 (.25 inches).

4.3 Force Signals

The balance-amplifier-visicorder system performed without fault. The major source of scatter in the force

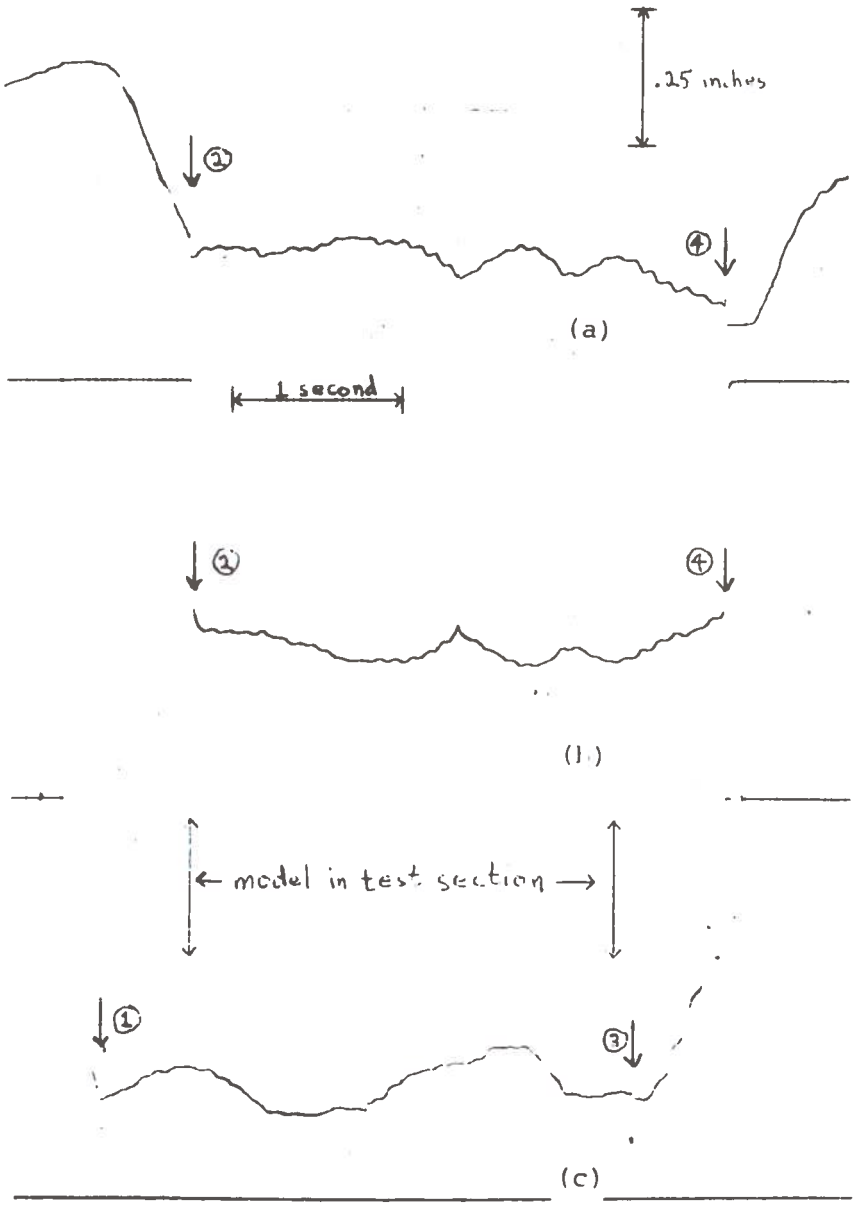

Fig. 4.1 Typical Chart Recording of Displacement Signals.
(a) Left Rear Transducer; (b) Right Rear Transducer;
(c) Forward (left) Transducer.

(1) Forward transducer enters test section.
(2) Rear transducers enter test section.
(3) Forward transducer exits test section.
(4) Rear transducers exit test section.

readings was the balance. Design repeatability is about 3% of the full scale load. However, the greatest forces recorded were all less than half of full scale. Side force and rolling moment are especially small when the model has no roll angle. The errors for typical forces on the model with no roll are 10% on lift, 80% on pitching moment (this corresponds to 3% of the chord in locating the center of pressure), 50% on rolling moment, 40% on side force, 25% on yawing moment and 15% on drag.

The major source of error in the balance is hysteresis in the strain gauges. The vibrations during testing would reduce the effects of hysteresis so that the accuracy may be better than that indicated by the static calibrations.

4.4 Pressure Signature

The pressure signature of the model suffered from the carriage vibrations. A typical pressure signal measured near the bottom of the guideway is shown in Figure 4.2. The sharp dip in the pressure signal matched with a sharp decrease in the drag signal. A non-constant forward speed of the model would cause the drop of pressure seen in the signature. Apparently, an irregularity in the carriage rails caused a jerk in the forward velocity that reproducibly interrupted the pressure signal.

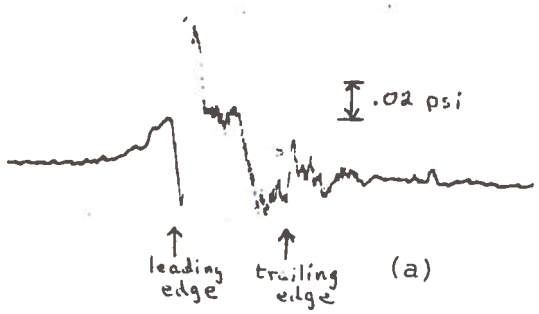

Fig. 4.2 Typical Chart Recording of Pressure Signals.

(a) Pressure transducer above lip plane (top hole in guideway).

(b) Pressure transducer near bottom of guideway.

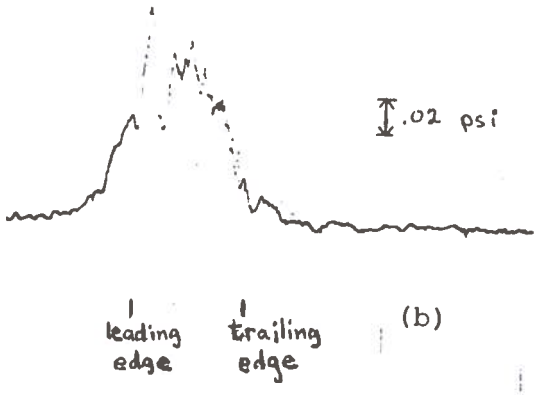

Fig. 4.3 Relative Location of Pressure and Displacement Transducers.

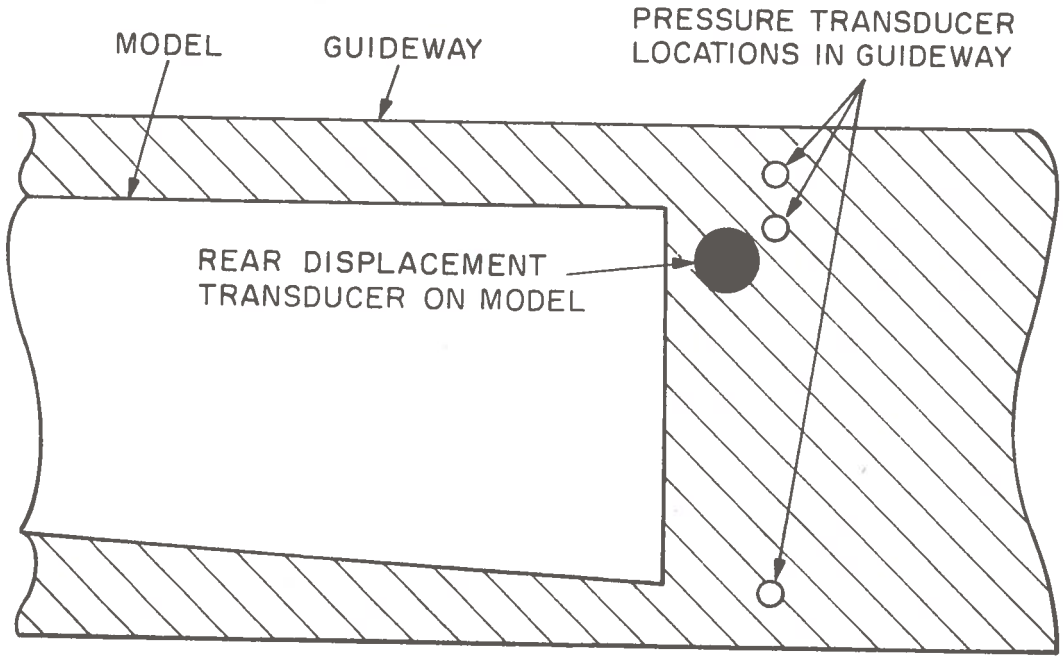

Near the trailing edge both the noise and pressure approached zero. Typically, the pressure at the trailing edge was greater than ambient, corresponding to a fluid velocity of .96 of the free stream value. There was no measurable variation of the trailing edge pressure due to angle of attack.

The pressure above the lip plane was measured on several runs when the angle of attack was 2.75 degrees. The average pressure corresponded to a contraction ratio of .87 for the flow through the gap. Near the trailing edge, the influence of the position transducer caused a high fluid velocity and negative pressure was recorded there. Figure 4.2 shows a typical pressure signal measured above the lip plane. Figure 4.3 is a schematic drawing of the relative position of the displacement transducer and the three locations for the pressure transducer.

4.5 Data

Lift and pitching moment are reported in Figures 4.4 to 4.7. The lift and pitching moment are considered independent of side displacement and yaw angle. The computed curve is the theory of Boccadoro: a numerical integration of one-dimensional mass conservation beneath the model. The governing equation is made one-dimensional by assuming spanwise constant pressure beneath the vehicle.

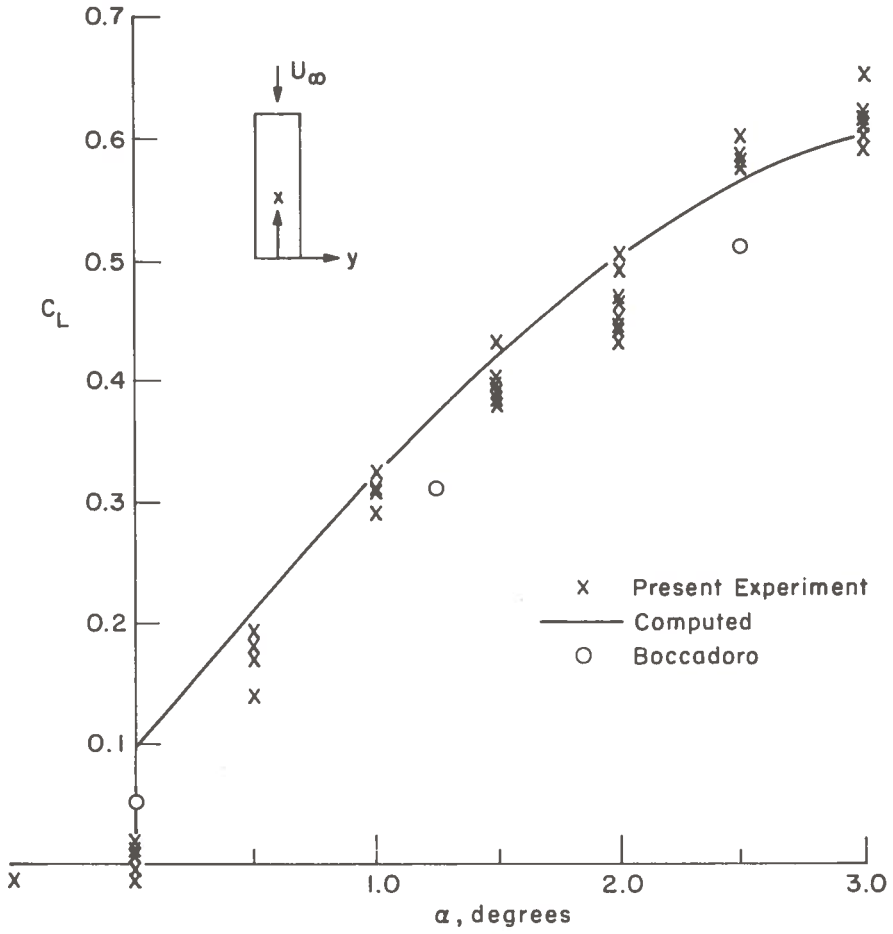

Fig. 4.4 Lift Coefficient vs. Angle of Attack
$\varepsilon = 0.087$

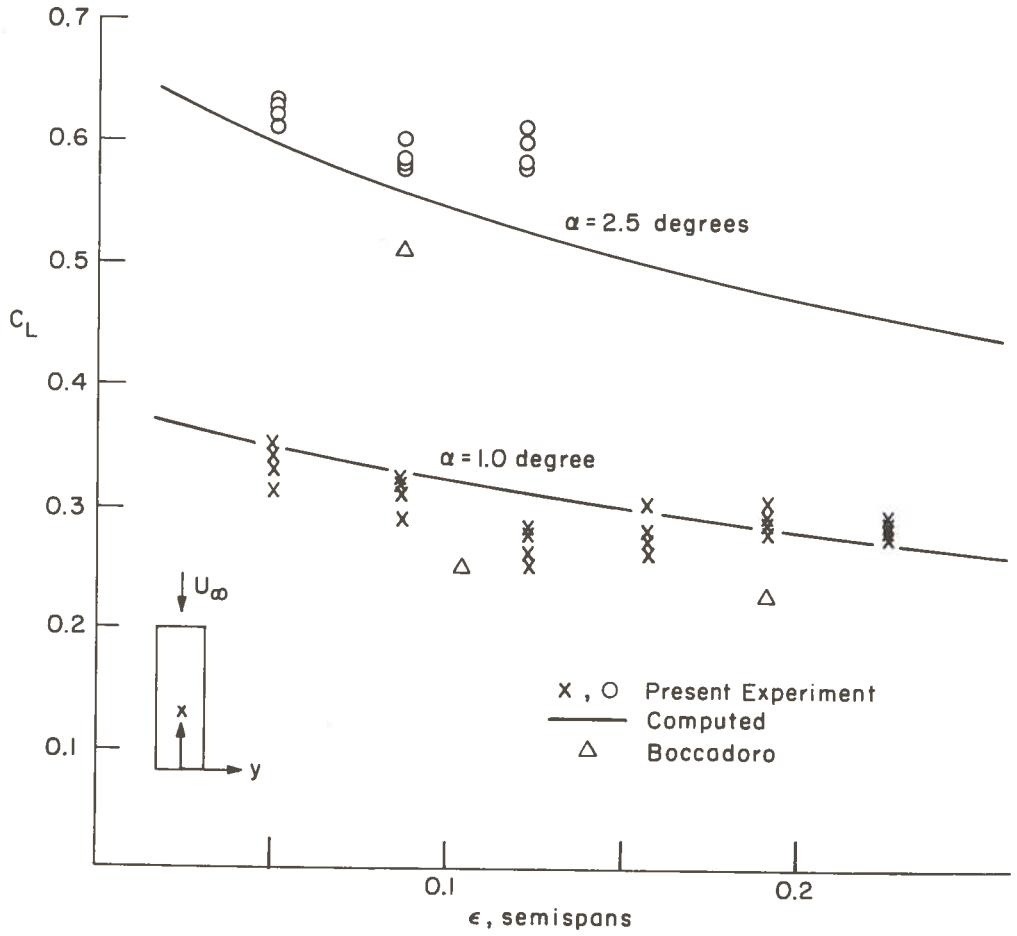

Fig. 4.5 Lift Coefficient vs. Clearance

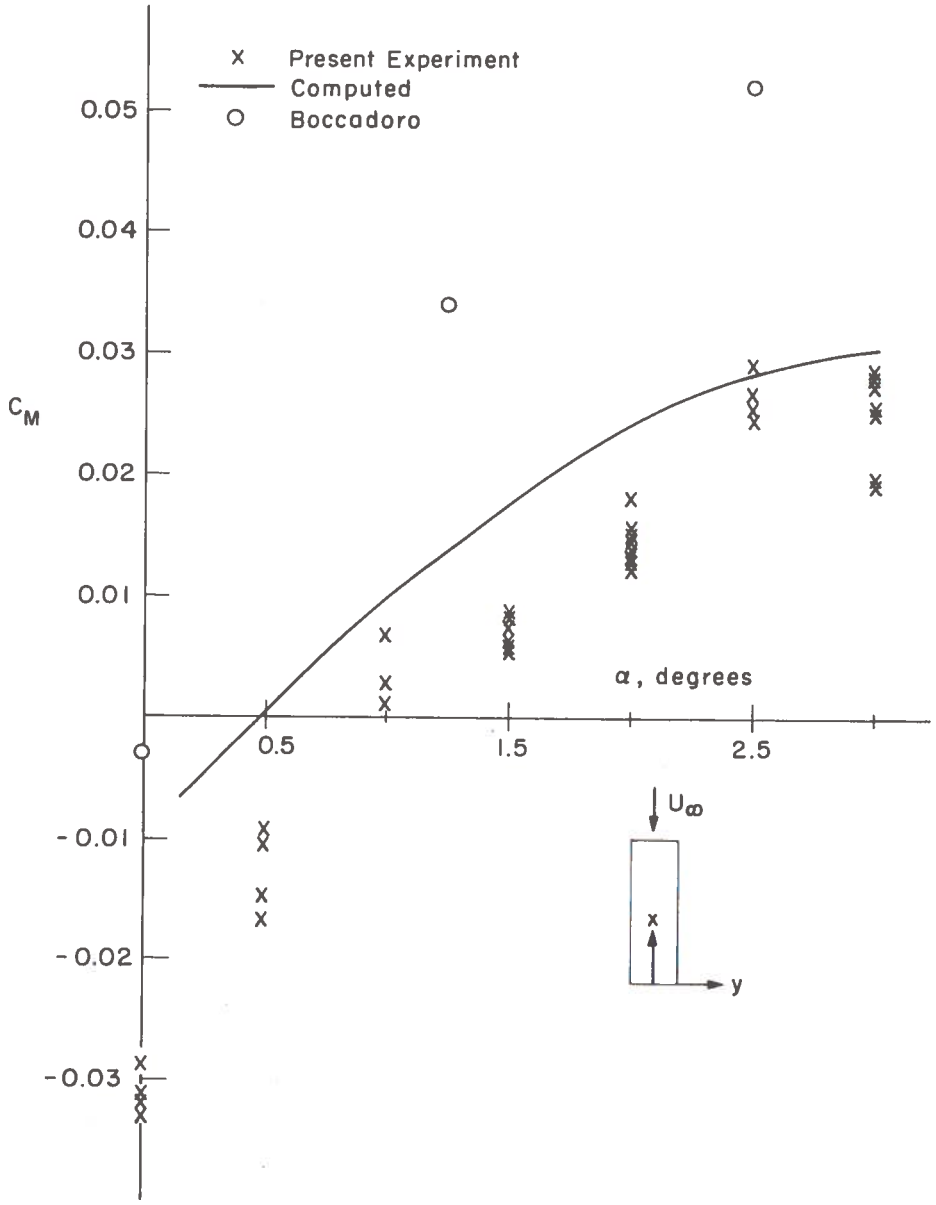

Fig. 4.6 Pitching Moment vs. Angle of Attack
$\varepsilon = 0.087$

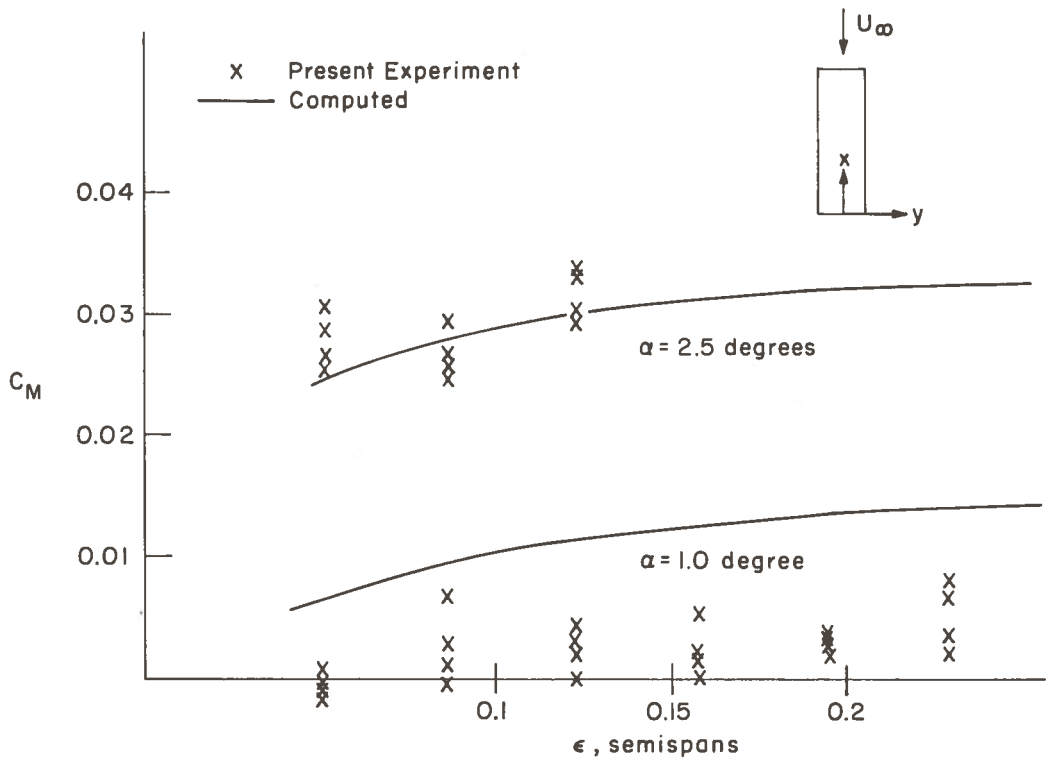

Fig. 4.7 Pitching Moment vs. Clearance

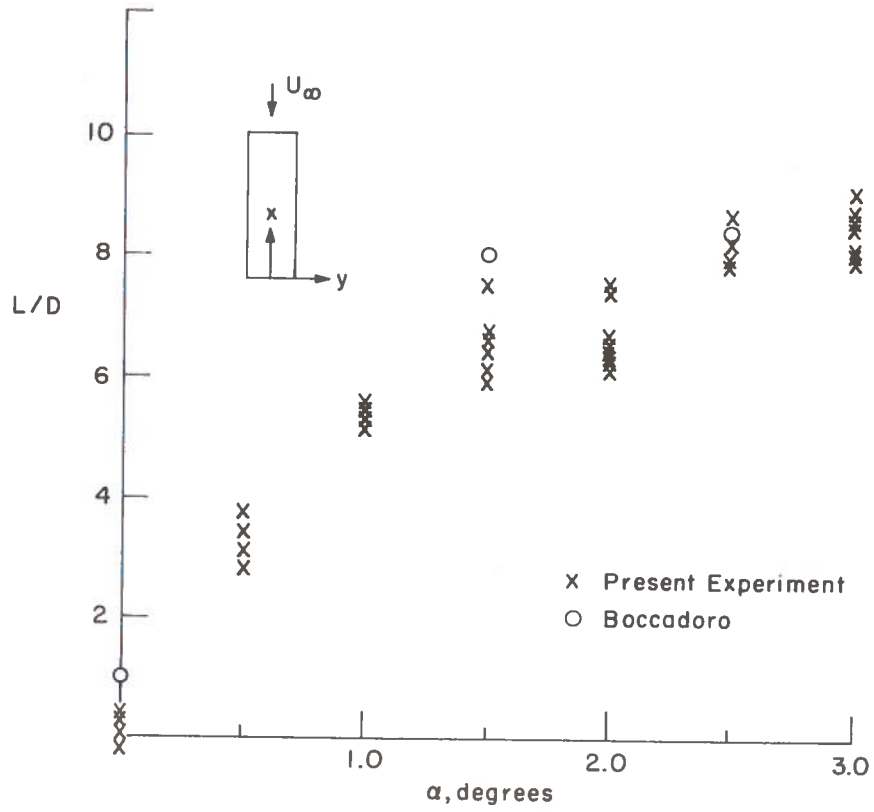

Fig. 4.8 Lift-to-Drag Ratio
vs. Angle of Attack
$\varepsilon = 0.087$

The numerical program uses a trailing edge velocity of .96 and a contraction ratio for the side gap of .87 as mentioned in Section 4.3. Good agreement is seen. Figure 4.8 shows the lift-to-drag ratio as a function of angle of attack. Drag was taken to be the sum of the induced drag and the drag measured by the balance (along the chord).

Three points from the data of Boccadoro are included in the figures. Direct comparison with the results of Boccadoro is difficult because of the different definitions of the clearance ratio ε. Boccadoro used ε_o, the vertical clearance at the midchord, as opposed to the trailing edge clearance used herein. The points used for comparison were taken from Boccadoro's original data, some of which were not reported in Reference 8. The difference is within experimental error, and both data show the same slope as a function of angle of attack. The current experiment uses different fairings and added the displacement transducers to the upper surface of the model.

To obtain the lateral derivatives, the force levels were plotted as a function of side displacement. Since the yaw angle varied for the different points, a "correction" for the rolling moment due to yaw angle was assumed in order to improve the data such that a least-squares straight line could be fitted on the plot. The slope of the line is taken

as the side displacement derivative and the "correction" for yaw angle is the yaw angle derivative. This process is repeated for various angles of attack and clearances. Appendix C discusses the data reduction procedure in more detail.

Figures 4.9 and 4.10 show the rolling moment and side force due to side displacement as a function of angle of attack. The prediction is from the analysis of Chapter 2. Side displacements up to $0.5\lambda_o$ occurred in the experiment. The data reduction process did not allow for non-linearities (see Appendix C). Thus, part of the data scatter could be due to non-linear effects. In Figure 4.9, the two predicted curves are for $\varepsilon = 0.087$ and $\varepsilon = 0.123$ for $\lambda = 0$:

$$C_{\ell_\lambda}\Big)_{\substack{\varepsilon = 0.087 \\ \lambda = 0}} = -.327\alpha - .257 \qquad (4.1)$$

$$C_{\ell_\lambda}\Big)_{\substack{\varepsilon = 0.123 \\ \lambda = 0}} = -.310\alpha - .216 \qquad (4.2)$$

Both predicted curves show a greater magnitude than the data. The slope of the predicted curves agrees with the data, especially for smaller angles of attack. If side displacements greater than $\lambda = 0$ are considered, agreement of theory and data is aggravated, since non-linear effects increase the magnitude of the prediction. In Figure 4.10, the predicted curves are given by:

$$C_{y_\lambda}\Big)_{\substack{\varepsilon = 0.087 \\ \lambda = 0}} = -.318\alpha - .370 \qquad (4.3)$$

$$C_{y_\lambda}\Big)_{\substack{\varepsilon = 0.123 \\ \lambda = 0}} = -.254\alpha - .330 \qquad (4.4)$$

Good agreement is seen for $\varepsilon = 0.087$. For $\varepsilon = 0.123$, the data shows increasing magnitude for increasing clearance, while the theory predicts decreasing magnitude for increasing clearance.

The analysis of Chapter 2 is obviously inappropriate for the model with a keel. A keel would restrict crossflow beneath the model, resulting in a greater pressure difference between the two sides of the model. The keel affects the rolling moment much more than the side force. Since the keel is below the roll axis, the pressure on the keel contributes a rolling moment opposite that from the pressure on the model body. However, the area of the keel is much less than the area of the model body and a net increase in rolling moment results. It could be expected that the side force is less affected by the keel since the fluid velocities at the sides of the model are somewhat independent of each other. Figures 4.9 and 4.10 also show that for decreasing clearance the magnitude of C_{ℓ_λ} increases while the magnitude of C_{y_λ} changes little. This again indicates that the conditions of crossflow affect C_{ℓ_λ} more than C_{y_λ}.

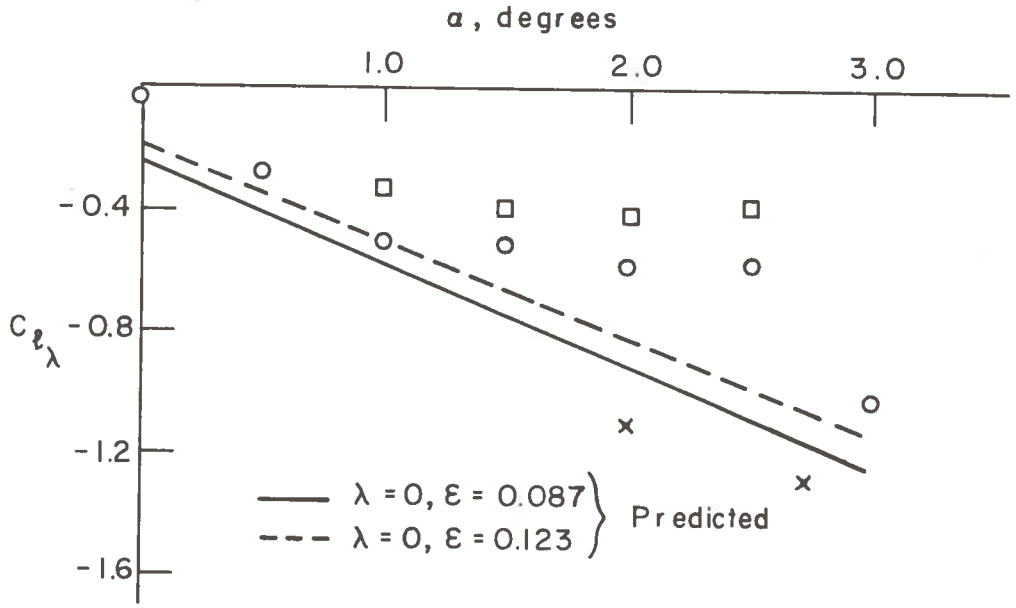

Fig. 4.9 Rolling Moment Due to Side Displacement vs. Angle of Attack

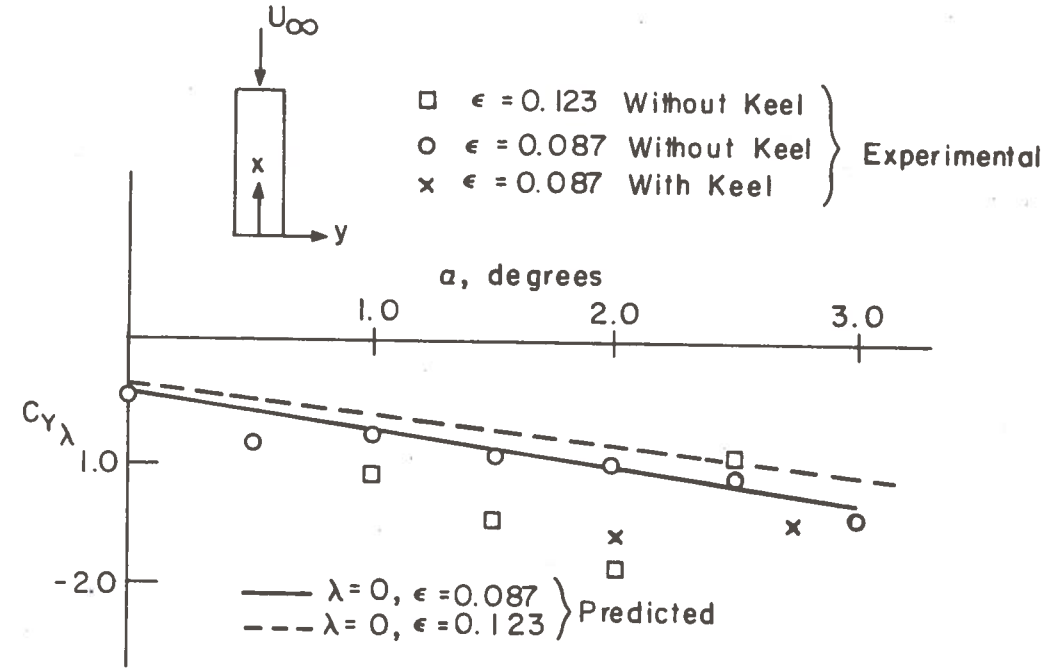

Fig. 4.10 Side Force Due to Side Displacement vs. Angle of Attack

Figures 4.11 and 4.12 present the rolling moment and side force due to yaw angle. The two predicted curves in Figure 4.11 represent the range of C_{ℓ_ψ} if side displacements up to $0.5\lambda_o$ are considered, with the yaw angle taken as zero:

$$C_{\ell_\psi}\Big)_{\substack{\lambda = 0 \\ \psi = 0}} = .273\alpha + .66 \tag{4.5}$$

$$C_{\ell_\psi}\Big)_{\substack{\lambda = 0.5\lambda_o \\ \psi = 0}} = .460\alpha + 3.06 \tag{4.6}$$

Most of the data fits the prediction for $\lambda = 0.5\lambda_o$, with the curve for $\lambda = 0$ providing a range for C_{ℓ_ψ} that includes the data points for higher angles of attack. The small effect of the keel seen in Figure 4.11 suggests that the forces due to yaw arise principally from the flow at the sides of the model. This was verified in the process of deriving Equations (4.5) and (4.6) in which it was seen that the major contribution to the moment came from the integral of the circulation at the sides of the model.

The side force due to yaw is seen to fit the analytical prediction for low angles of attack if side displacements up to $.25\lambda_o$ are considered (yaw angle taken as zero):

$$C_{y_\psi}\Big)_{\substack{\lambda = 0 \\ \psi = 0}} = 1.10\alpha + 1.86 \tag{4.7}$$

$$C_{y_\psi}\Big)_{\substack{\lambda = 0.25\lambda_o \\ \psi = 0}} = 1.18\alpha + 2.31 \tag{4.8}$$

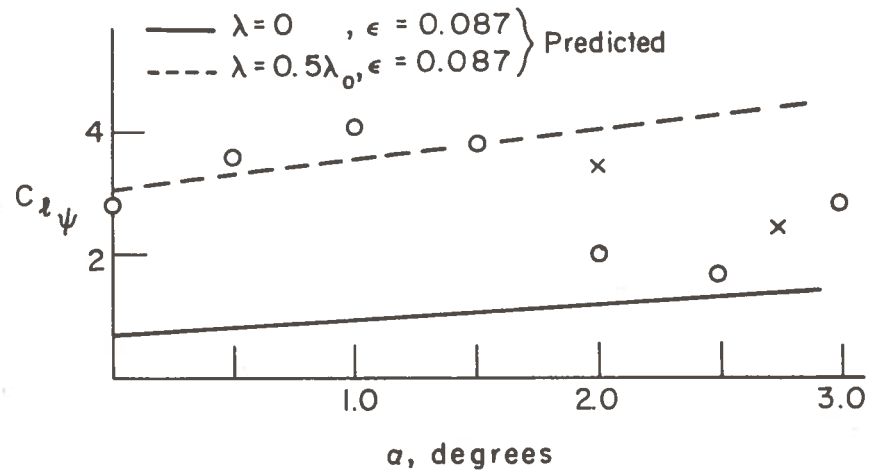

Fig. 4.11 Rolling Moment Due to Yaw vs. Angle of Attack

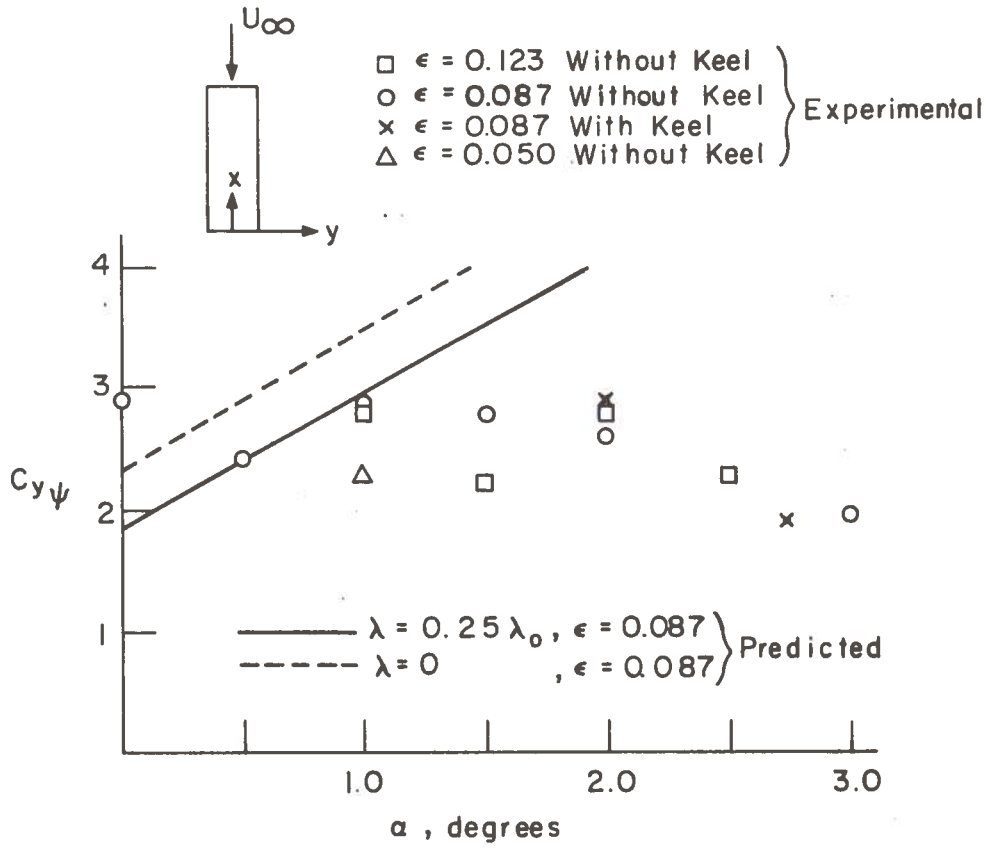

Fig. 4.12 Side Force Due to Yaw vs. Angle of Attack

It was seen in Equation (2.8) that the major influence of yaw angle on side force was to change the side displacement at the trailing edge by $-\psi(c/2)$. Thus the slope of the prediction of C_{ℓ_ψ} should be $-(c/2)$ times the slope of the prediction of C_{ℓ_λ}. This is found to be so, although Figure 4.12 shows that it results in poor agreement with the data for C_{y_ψ} at larger angles of attack. As discussed in Chapter 2, asymmetrical flow separation at the sides of the model could be expected for asymmetrical configurations. For a yawed vehicle, the side displacement due to yaw at the trailing edge is opposite of that at the leading edge. Thus the difference in circulation at the two lips of the vehicle would have a chordwise variation. This effect would be greater at higher angles of attack (i.e., greater lift), where Figure 4.12 shows the trailing edge analysis to be in poor agreement with the measured values of C_{y_ψ}. The small effect of the keel and the vertical clearance shows that side force due to yaw arises principally from the flow at the sides of the model.

Rolling moment and side force due to roll are reported in Figures 4.13 and 4.14. The rolling moment is seen to be stabilizing, increasing with higher angle of attack. The keel is seen to have little influence, suggesting that the roll angle causes little crossflow. However, in body axes, the roll axis is inclined to the ground with the angle of

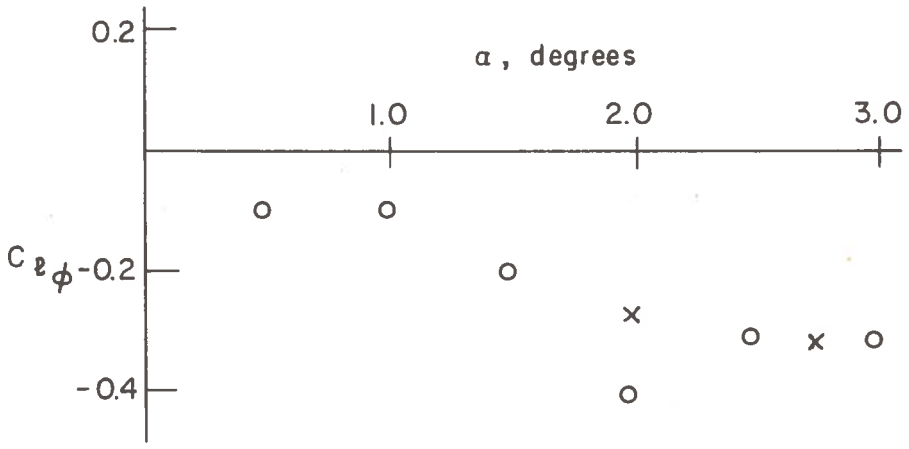

Fig. 4.13 Rolling Moment Due to Roll vs. Angle of Attack

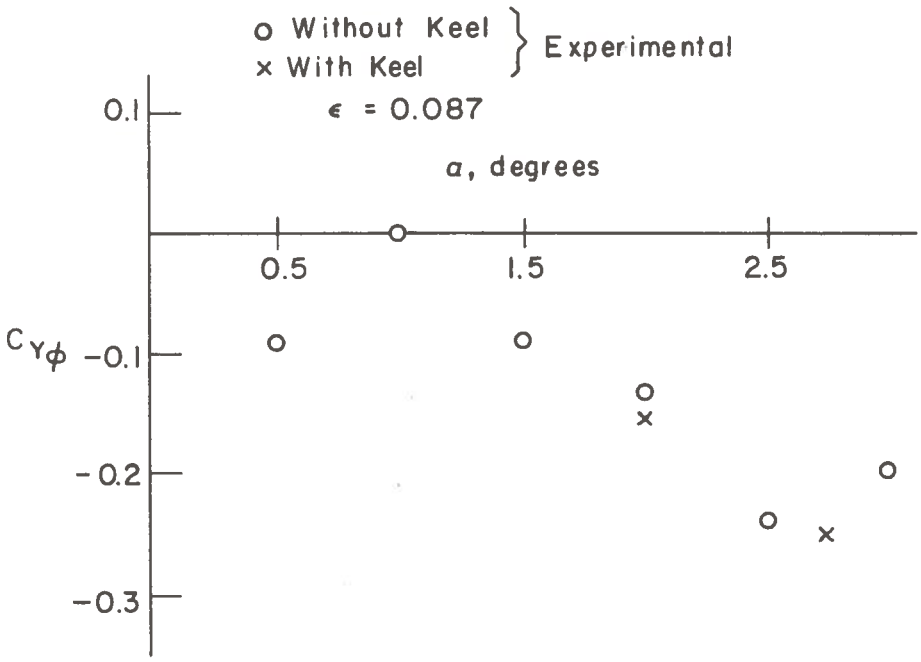

Fig. 4.14 Side Force Due to Roll vs. Angle of Attack

attack. Thus the keel is displaced sidewards and up, especially near the leading edge where larger pressure differences beneath the model occur. This would reduce the effectiveness of the keel to restrict crossflow beneath the model.

When the model is rolled, the side displacement measured in the lip plane is held constant. This is the same as if the roll axis were in the lip plane, although the roll axis in the force balance is near and parallel to the bottom of the model.

Figures 4.15 and 4.16 present the yawing moment due to side displacement and yaw angle. For side displacement alone, no chordwise variation in the sidegap occurs. Thus little yawing moment should result, as is seen in Figure 4.15. For a yawed vehicle, the chordwise variation in the sidegap should produce a yawing moment, which is seen to be stabilizing for non-zero angle of attack in Figure 4.16.

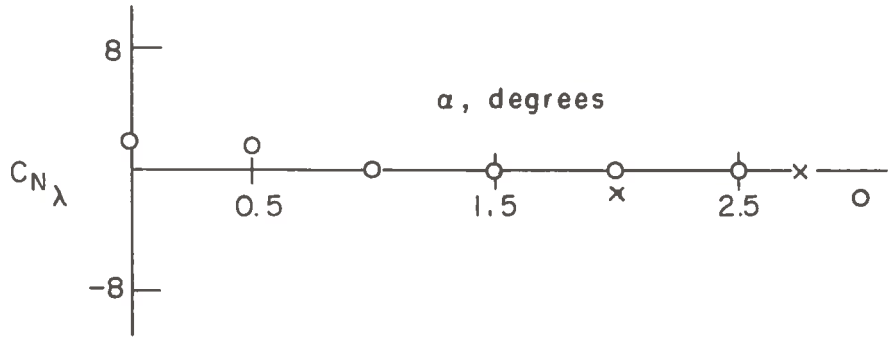

Fig. 4.15 Yawing Moment Due to Side Displacement vs. Angle of Attack

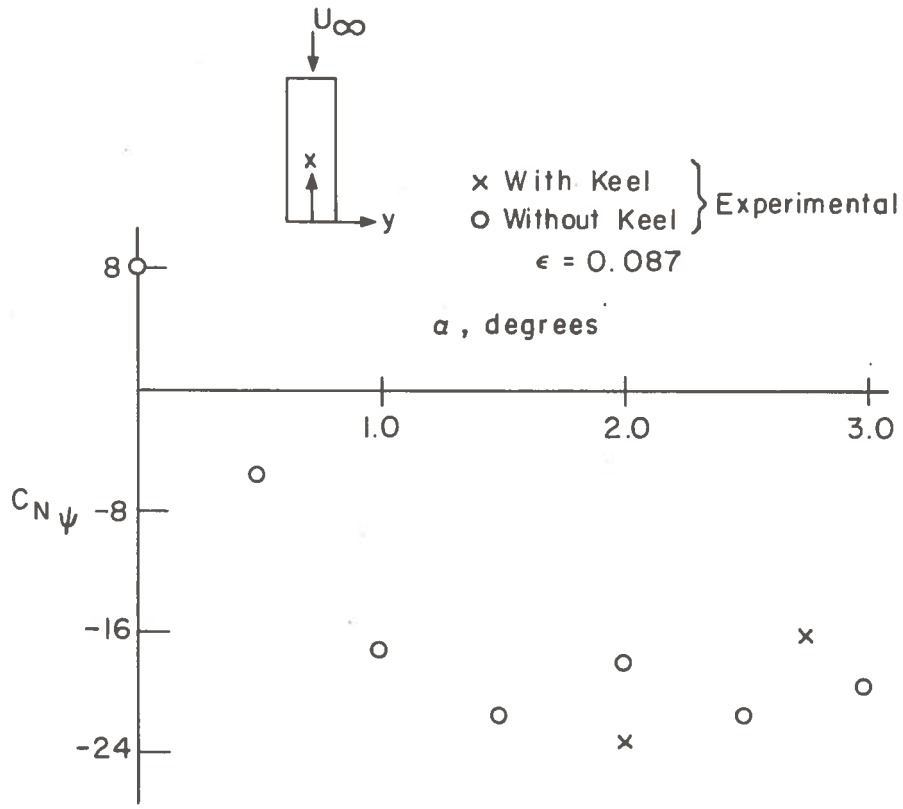

Fig. 4.16 Yawing Moment Due to Yaw vs. Angle of Attack

5. CONCLUSIONS

The results show the dynamic ram air cushion vehicle can be considered as a candidate for high-speed ground transportation. The primary lateral derivatives are all stabilizing. Side displacement generates a restoring side force coupled with a rolling moment but no yawing moment. Roll angle generates a restoring rolling moment coupled with a side force. (Yawing moment due to roll was not evaluated). Yaw angle generates a restoring yawing moment coupled with a side force and a rolling moment.

The keel has a significant effect only on C_{ℓ_λ}, indicating that crossflow beneath the model is not important for side force or yawing moment and that the rolling moment due to yaw angle is dominated by pressures acting at the sides of the vehicle.

The lift coefficient was as large as .6 at 3.0 degrees angle of attack and zero for zero angle of attack. The pitching moment was positive (nose up) over most angles of attack but was negative for zero and 0.5 degrees angle of attack. The center of pressure did not vary more than 5% from the midchord.

Boccadoro's numerical procedure provides a good prediction of the lift and pitching moment, especially at larger angles of attack. The prediction of the lateral derivatives using a trailing edge Trefftz analysis showed good aggreement with the data for side displacement. The range of the data for rolling moment due to yaw was predicted successfully, but the measured side force due to yaw fitted the predicted range only for small angle of attack. The prediction of the lateral forces due to roll angle was completely unsuccessful.

Further improvement to the Trefftz analysis presented here should focus on determining the value of the circulation at the lips of the vehicle. Apparently the imposition of zero circulation at the lips of the model does not seriously jeopardize the prediction of side displacement derivatives. The lesser success of predicting the yaw angle derivatives and the failure of predicting the roll angle derivatives show where more detailed analysis is needed. Three-dimensional analysis is obviously required to predict the yawing moment, and may also be necessary to accurately predict the side force and rolling moment due to yaw, especially at larger angles of attack.

As one can see in Appendix A, the trailing edge Trefftz analysis does not require the ordering assumptions that are necessary for previous pertubation expansion

analyses. A proper evaluation of the accuracy of the Trefftz analysis would require a better controlled experiment than that reported here. In particular, the crooked path of the model gives rise to yaw rate and side displacement velocity that would affect the "sidewash" used in the analysis.

As an experimental technique the towing tank should become a valuable tool in the study of dynamic air cushion vehicles. The need for accuracy in guideway alignment and monitoring the model position is common to all methods of testing vehicles in a guideway. The towing tank has the advantage of automatically simulating the ground and guideway walls for both static and dynamic model configurations. For example, the yaw angle derivatives for this experiment were obtained because the yaw angle differed at various locations in the guideway. Installing several sections of the guideway at a yaw angle with respect to the model path could be used to measure the effect of yaw rate. Future tests will be able to take more complete advantage of the benefits of the towing tank method

It was expected at the outset that the towing tank method would involve difficulties, and it can be said in fairness that these tests encountered their full share of troubles. In spite of this, all of the major experimental

goals were accomplished. All indications are that the technique is conceptually sound and can serve a useful role investigating the aerodynamics of high speed ground transportation vehicles in general.

APPENDIX A

TREFFTZ ANALYSIS OF FLAT PLATE WITH ROLL

Figure A.1 shows the Trefftz plane flow for a flat plate with a roll angle over an infinite ground plane. From mass continuity, the velocity in the region beneath the wing is the cumulative downwash divided by the height of the region:

$$V(y) = \frac{w_o y + w_o K_1}{h(y)} \tag{A.1}$$

where k_1 is a constant of integration. Let $\sin\phi = \phi$ and $\bar{\phi} = \phi/\varepsilon$. Then $h(y) = \varepsilon(1 + \phi y)$ and

$$\Gamma(y) = -\frac{1}{\varepsilon}\int^{y} \frac{w_o y + w_o k_1}{1 + \bar{\phi} y}\, dy + K_2$$

The constants K_1 and K_2 are evaluated with the boundary conditions $\Gamma(\pm 1) = 0$ to obtain the result:

$$\Gamma_{(y)} = \frac{w_o}{\varepsilon\bar{\phi}^2}\left[\log(1+\bar{\phi}y) - \frac{y}{2}\log\left(\frac{1+\bar{\phi}}{1-\bar{\phi}}\right) - \frac{1}{2}\log(1-\bar{\phi}^2)\right] \tag{A.2}$$

Expanding the log terms,

$$\Gamma_{(y)} = \frac{w_o}{2\varepsilon}\left[(1-y^2) + \frac{2\bar{\phi}}{3}(y^3-y) + \frac{\bar{\phi}^2}{2}(1-y^4) + \ldots\right] \tag{A.3}$$

The first term gives the lift of a flat plate with no roll. The second term generates a restoring rolling moment, and the third term shows the additional lift due to roll. Equation (A.2) is correct for all roll angles if ϕ is replaced by sin ϕ.

It is a simple procedure to calculate the restoring rolling moment on the wing from Equation (A.3):

$$C_\ell = \frac{1}{c}\int_{-1}^{1} y\Gamma dy = -\frac{4\bar{\phi}w_o}{45\varepsilon c} \qquad (A.4)$$

Barrows (10) has derived the rolling moment on a rolled plate in a trough using the method of matched asympotic expansions. His expression for the rolling moment includes a contribution from the side gap effects (i.e., $\Gamma \neq 0$ at $y = \pm 1$). If the side gap contribution is neglected, Equation (A.4) is identical to Barrows result.

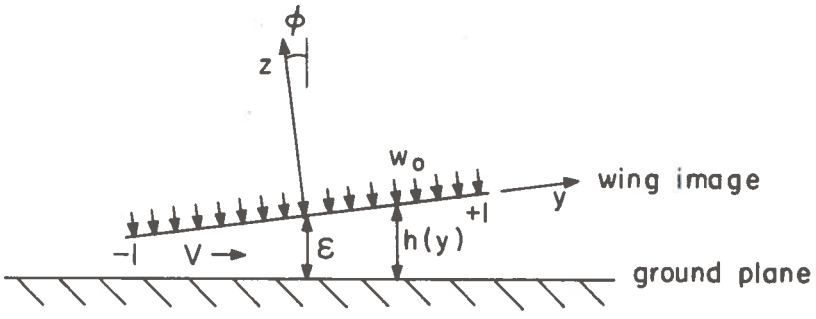

Fig. A.1 Trefftz Plane Flow

APPENDIX B

CORNER FLOW MAPPING

The flow at the corner of the model can be mapped using a Schwarz-Christoffel transformation as sketched in Figure B.1. The derivation can be found in various references, for example, (14). The transformation for Figure B.1 is

$$Z = \frac{2\varepsilon}{\pi}\tanh^{-1}\left(\frac{1-\zeta/\omega}{1+\zeta}\right)^{1/2} - \frac{2\Lambda}{\pi}\tan^{-1}\left(\frac{\omega-\zeta}{1+\zeta}\right)^{1/2} - 1 \qquad (B.1)$$

with $\omega = \varepsilon/\Lambda$. For a unit source at $\zeta = 0$, the velocity in the Z-plane is

$$Q(Z) = -\left(\frac{\zeta+1}{\varepsilon^2-\Lambda^2\zeta^2}\right)^{1/2} \qquad (B.2)$$

At the corner of the model, $\zeta = \varepsilon^2/\Lambda^2$ and

$$Q(Z) = -\left(\frac{9}{4\pi}\right)^{1/3} \varepsilon^{2/3} (\varepsilon^2/\Lambda^2 + 1)^{1/3} (Z+1)^{-1/3} \qquad (B.3)$$

as $Z \to -1$. This singularity can be integrated to give an average velocity near the corner. It is not appropriate to extend equation (B.3) completely across the channel, but it does indicate the impedance seen by the flow as it turns the corner.

The analysis of Chapter 2 for side displacement uses a velocity constant across the channel with a discontinuity

in velocity at the corners ($y = \pm 1$ in Figure 2.2). The velocity in the side gaps predicted by averaging equation (B.3) is compared to the velocity in the side gaps derived from the analysis of Chapter 2 in Table B.1.

Table B.1

r	J	$J\frac{(1 - r)}{(1 + r)}$	$\frac{(1 - r)}{(1 + r)}$
0	1	1	1
1/4	1.07	.64	.60
3/8	1.10	.50	.45
1/2	1.14	.38	.33

$$J = \frac{(s^2(1 + r)^2 + 1)^{1/3}}{(s^2(1 - r)^2 + 1)^{1/3}} \quad \text{with } s = \lambda_o/\varepsilon = 1/2,\ r = \lambda/\lambda_o$$

$$J\frac{(1 - r)}{(1 + r)} = \frac{\text{velocity in } \lambda_L}{\text{velocity in } \lambda_R} \quad \text{from equation (B.3)}$$

$$\frac{(1 - r)}{(1 + r)} = \frac{\text{velocity in } \lambda_L}{\text{velocity in } \lambda_R} \quad \text{from Chapter 2 analysis}$$

The values of r and s used in Table B.1 represent the range of the parameters encountered in the experiment. The results indicate that the analysis of Chapter 2 is adequate to derive the circulation on the model within 14%.

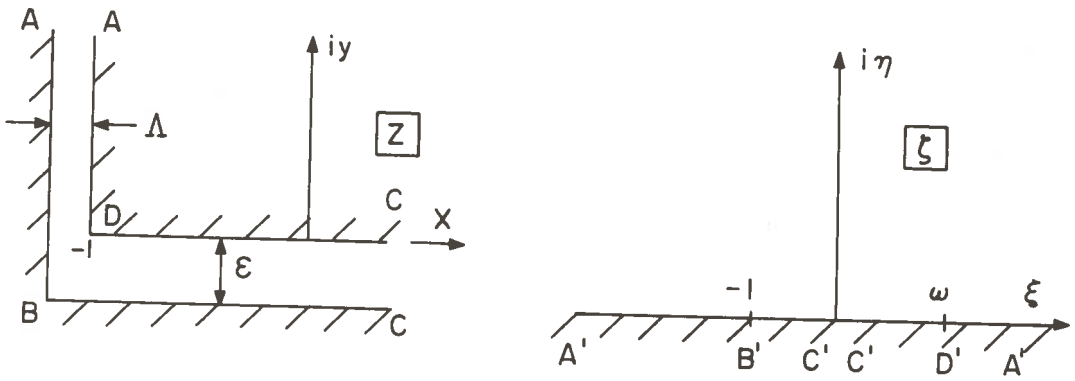

Fig. B.1 Corner Flow Mapping

APPENDIX C

DATA REDUCTION

As discussed in Sections 3.1 and 3.2, the path of the model in the guideway was not straight due to misalignment of the carriage rails. Thus the side displacement and yaw angle of the model varied continuously through the test section. Data was sampled at two intervals of the test section, one near the center and the other near the exit. The model position and forces were averaged over the length of the interval, the length of the interval being chosen such that the elapsed time equaled three time constants of the filter averaging circuit (one second).

The lift and pitching moment were taken to be independent of side displacement and yaw angle. Thus this data was taken directly from the force recordings. The lateral forces, however, always included an interaction between the effects of side displacement and yaw angle.

To obtain the lateral derivatives, the force levels were plotted as a function of side displacement. Figure C.1 is an example of the rolling moment. Since the yaw angle varied for the different points, its influence obscures the effect of the side displacement acting alone. In order to separate out the effects of yaw angle, a value for

C_{ℓ_ψ} was assumed and the data points were "corrected" for the amount of yaw angle included in each point. The value of C_{ℓ_ψ} was varied until a least-squares best fit was obtained with a straight line through the corrected data. Figure C.2 shows the result for C_ℓ vs. λ from the data of Figure C.1. The slope of the line fitted to the data points of Figure C.2 is taken to be C_{ℓ_λ}. This process is repeated for the various angles of attack and clearances.

The same procedure was used to obtain the side force derivatives. Side force was plotted as a function of side displacement and a value of C_{Y_ψ} was found such that a straight line would best fit the points. The slope of the resulting straight line was taken to be C_{Y_λ}

For the roll derivatives, the data was again plotted as a function of side displacement. The effect of yaw angle was taken to be the same as for the model with no roll, and the data corrected appropriately. To evaluate the effect of roll, a value for C_{Y_ϕ} (or C_{ℓ_ϕ}) was found such that a least-squares straight line through the data points gave the same value for C_{Y_λ} (or C_{ℓ_λ}) as for the model with no roll. This procedure assumes that C_{Y_λ}, C_{Y_ψ}, C_{ℓ_λ} and C_{ℓ_ψ} do not change when the model is at a roll angle. To find the side force due to roll angle, it was necessary to subtract out the component of lift that was included in the output of the side force balance (i.e. $L\sin\phi$), since the force balance remained parallel to the ground when the model was rolled.

To determine the yawing moment due to side displacement and yaw angle, the data reduction procedure was slightly modified: yaw angle was used as the independent variable and a correction for side displacement was found such that a least-squares straight line would best fit the data points. The side displacement correction gave C_{N_λ} and the slope of the resulting line gave C_{N_ψ}.

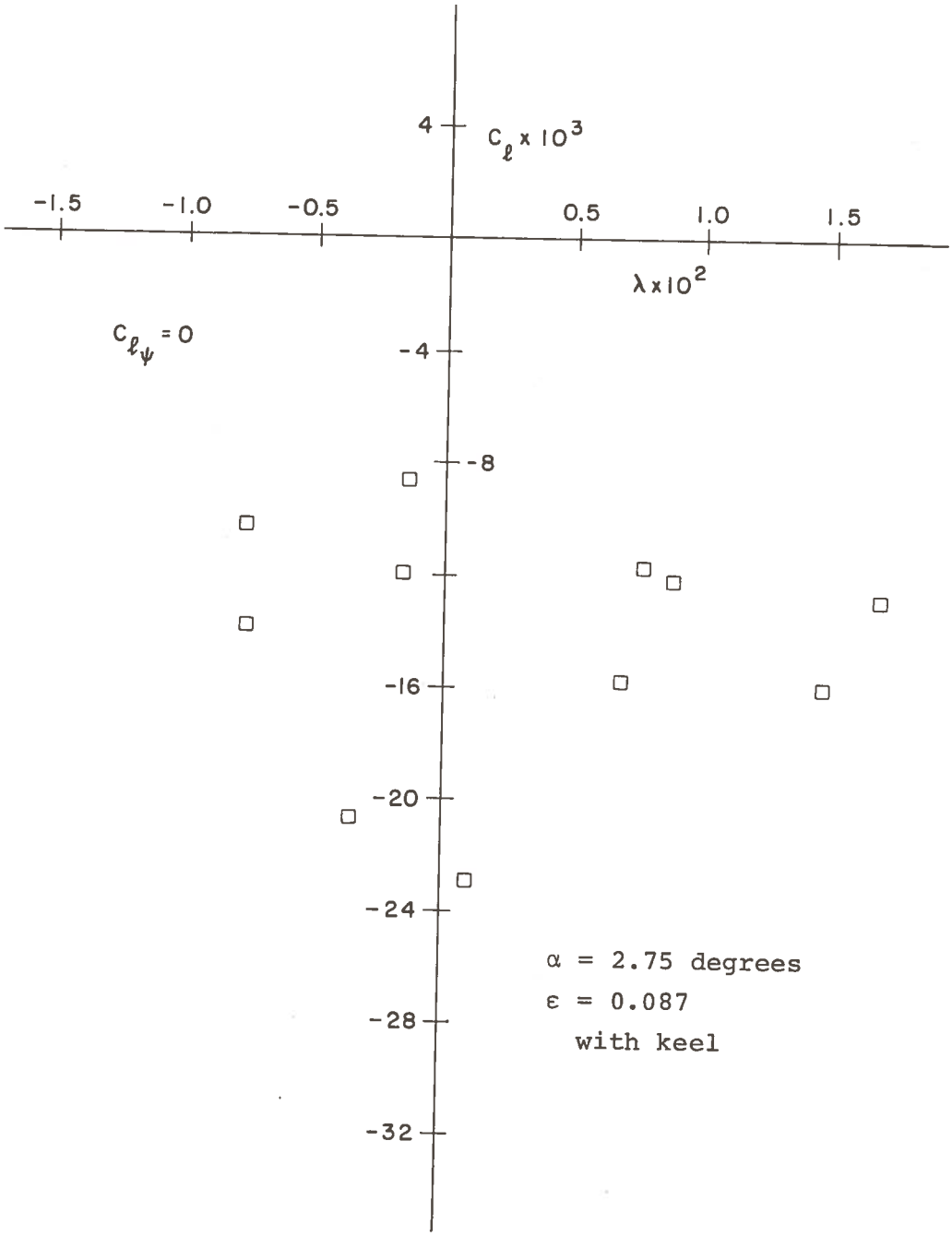

Fig. C.1. Rolling Moment vs. Side Displacement, No Correction for Yaw Angle (C_{ℓ_ψ} taken to be zero)

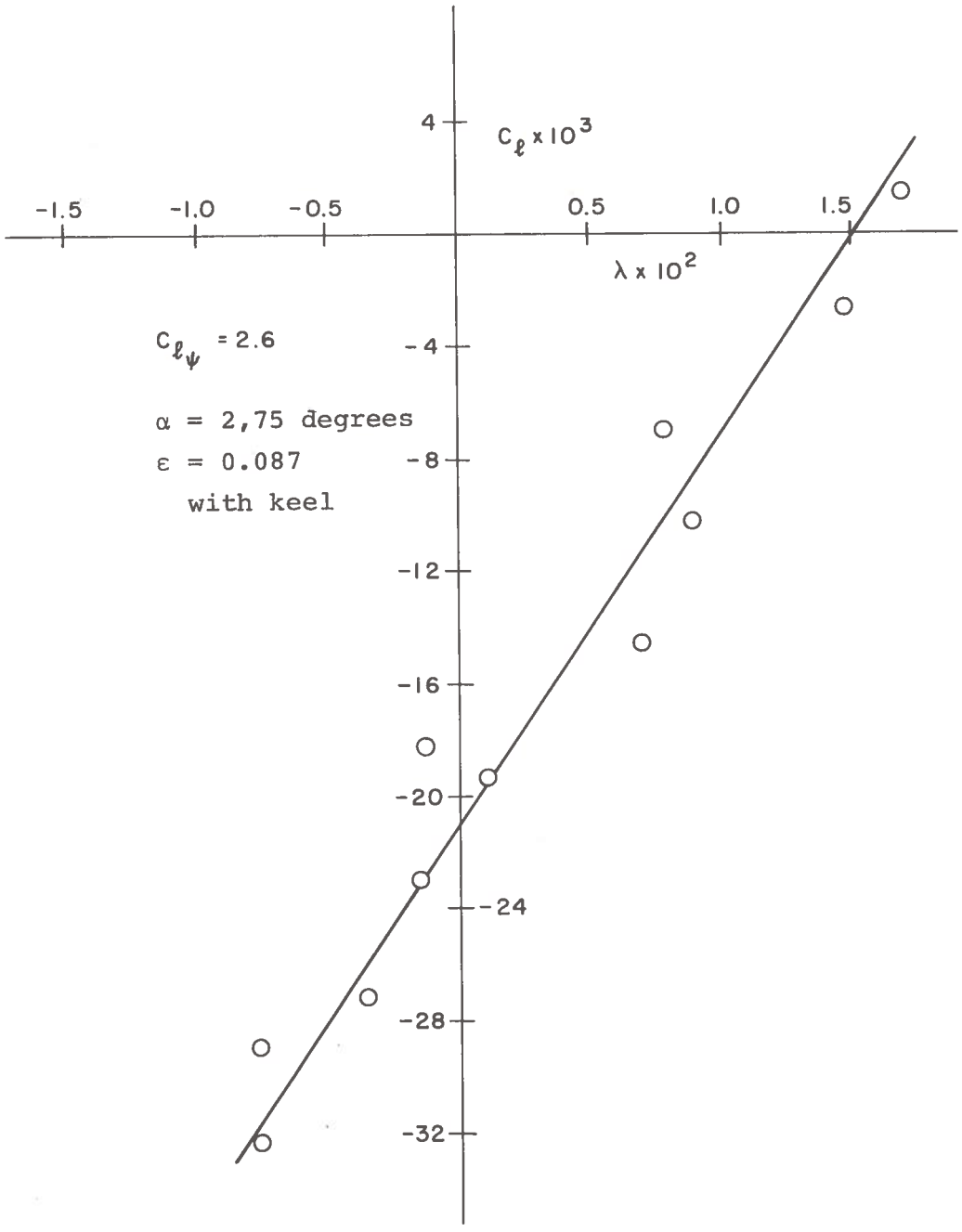

Fig. C.2. Rolling Moment vs. Side Displacement, Corrected for Yaw Angle (C_{ℓ_ψ} taken to be 2.6)

APPENDIX D

SIGNAL PROCESSING

As mentioned in Chapter 3, changes for this experiment focused on more accurate measuring of model position and force levels. In addition, a pressure transducer was installed in the guideway to record the pressure signature of the model.

The position sensors discussed in Chapter 3 were three Kaman Sciences, Model 1105-6C, eddy current displacement transducers. The transducers were .75 inches in diameter and approximately 2.5 inches long. The output voltage of their linear range was 0-1.0 volts and was recorded directly on a Hewlett-Packard, Model 7700, chart recorder.

For the force balance, a voltage regulator was built to provide the bridge excitation to all of the strain gauges. The six output signals were amplified and filtered by a D.C. circuit and then attenuated at the input to the recording galvanometer. Figure D1 is a schematic drawing of the circuitry for one channel. The power supply was common to all six channels. The potentiometer at the input of the amplifier was used to

zero the strain gauges for no load conditions. The potentiometer at the output of the amplifier is a voltage divider that adjusts the signal level at the output (hence, the net gain as seen by the galvanometer). The 10K ohm resistance at the galvanometer attenuated the output signal to a safe level for the galvanometer. This allowed a relatively large signal between the towing carriage and the recorder so that cable noise would be minimized. The voltage divider at the output was adjusted so that the maximum expected signal level would not exceed the range of the recorder. The galvanometers were all type Honeywell M200-350, operating in a Honeywell Model 1150 Visicorder.

The pressure signature was measured with a Setra Model 240 .25 inch diameter pressure transducer. Transducer sensitivity was 25 volts/psi. The transducer was inserted in one end of a short (1.1 inches) piece of .125 inch inside diameter plastic tubing. The other end was inserted in one of three holes in one guideway wall. The holes were threaded so that a short bolt could seal the two holes not being used at any one time. The pressure signal was recorded directly on the same recorder as for the position transducers.

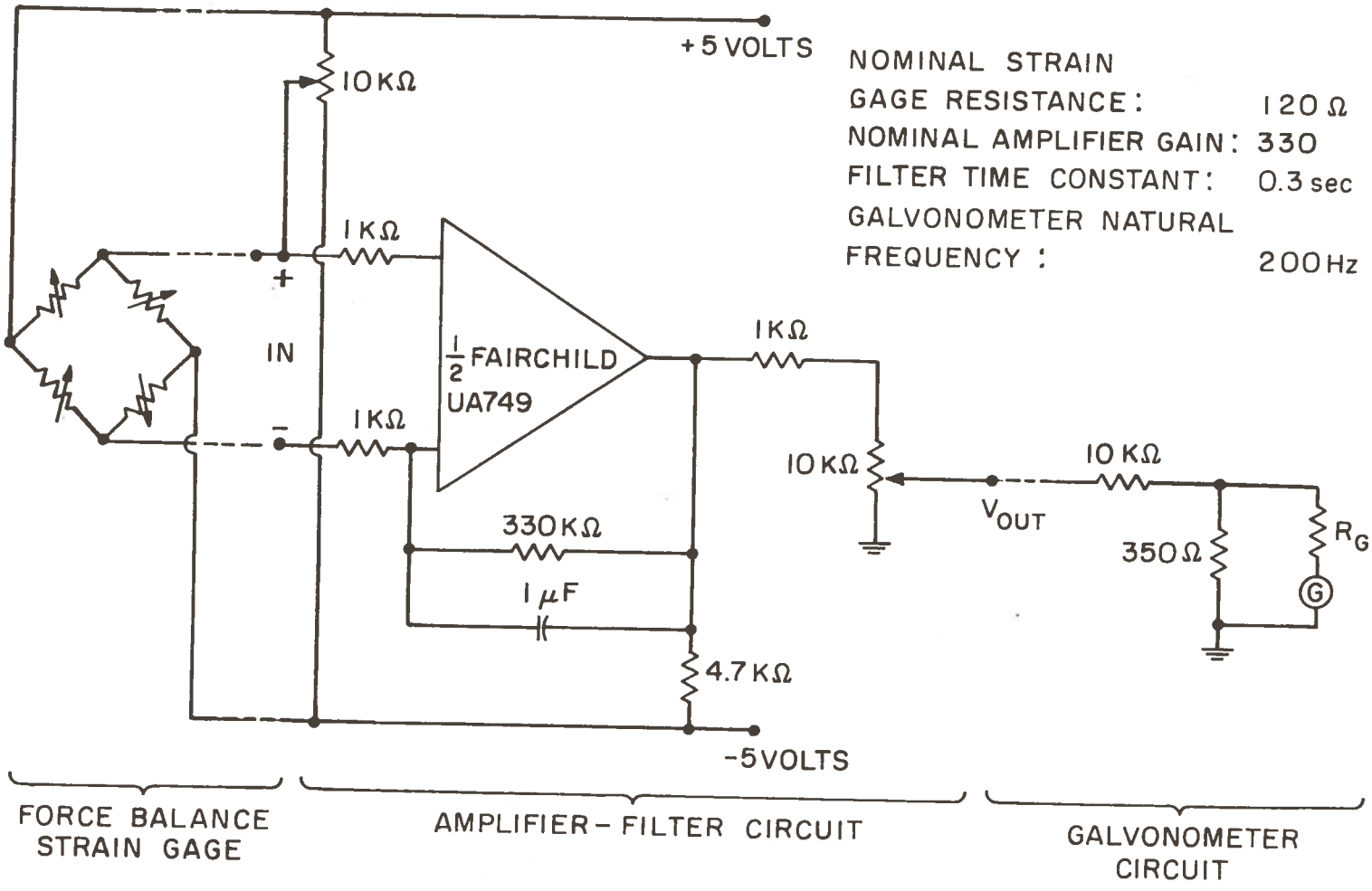

Figure D.1 Force Signal Circuit Schematic

APPENDIX E

REPORT OF INVENTIONS

After diligent review of the work performed under this contract (DOT-TSC-239), no new innovation, discovery, improvement or invention was made.

REFERENCES

1. Strand, T., W. W. Royce and T. Fujita, "Cruise Performance of Channel-Flow Ground-Effect Machine", Journal of the Aerospace Sciences, Vol. 29, No. 6, June, 1962, pp. 202-218.

2. Barrows, T. M., S. E. Widnall and H. H. Richardson, "The Use of Aerodynamic Lift for Application to High Speed Ground Transportation", Report FRA-RT-71-56, Acc. No. PB197-242, June, 1970.

3. Widnall, S. E. and T. M. Barrows, "An Analytic Solution for Two- and Three-Dimensional Wings in Ground Effect", Journal of Fluid Mechanics, Vol. 41, Part 4, 1970, p. 767.

4. Pepin, J. N., S. E. Widnall and T. M. Barrows, "An Experimental Study of a Flat-Bottomed Semi-Circular Wing in Very Close Proximity to the Ground", NASA Acc. No. N72-17003 or Report FRA-RT-72-23, Acc. No. PB203-602, September, 1971.

5. Pepin, J. N., "Study of a Ram Wing in a Trough", M.I.T. M.S. Thesis, 1970.

6. Gallington, R. W., M. K. Miller and W. D. Smith, "The Ram-Wing Surface Effect Vehicle: Comparison of One-Dimensional Theory with Wind Tunnel and Free Flight Results", NASA Acc. No. N71-36419, July, 1971 or Hovering Craft and Hydrofoil, Vol. 11, No. 5, 1972.

7. Boccadoro, Y. A., "Contribution to the Study of a Flat Bottomed Ram Wing Vehicle", M.I.T. E.A.A. Thesis, 1972.

8. Boccadoro, Y. A., "Towing Tank Tests on a Ram Wing in a Rectangular Guideway", Report FRA-RT-73-34, Acc. No. PB222-476, July, 1973.

9. Barrows, T. M., "Progress on the Ram Wing Concept with Emphasis on Lateral Dynamics", Report DOT-TSC-FRA-71-7, Acc. No. PB210-743, June, 1971.

10. Barrows, T. M., "Analytical Studies of Lift and Roll Stability of a Ram Air Cushion Vehicle", Report FRA-RT-73-21, Acc. No. PB219-820, December, 1972.

11. Matoi, T. K., "Lateral Stability Derivatives of a Ram Wing", M.I.T. M.S. Thesis, June, 1973.

12. Barrows, T. M. and S. E. Widnall, "Optimum Lift-Drag Ratio for a Ram Wing Tube Vehicle", AIAA Journal, Vol. 8, No. 3, 1970, p. 491.

13. Thwaites, B., Incompressible Aerodynamics, Oxford University Press, Oxford, 1960, Section VIII.12.

14. Morse, P. M. and H. Feshbach, Methods of Theoretical Physics, McGraw-Hill Book Co., Inc., New York, 1953, p. 1250.

15. Fraize, W. E. and T. M. Barrows, "The Tracked Ram Air Cushion Vehicle, A System Definition Study", PB230485, November, 1973.